Internodal excitonic state in a Weyl semimetal in a strong magnetic field

René Côté, Gautier D. Duchesne, and Santiago F. Lopez
Département de physique and Institut Quantique, Université de Sherbrooke, Sherbrooke, Québec, Canada J1K 2R1

(Received 22 April 2024; revised 19 June 2024; accepted 15 July 2024; published 31 July 2024)

The simplest Weyl semimetal with broken time-reversal symmetry consists of a pair of Weyl nodes located at wave vectors $\mathbf{K}_\tau = \tau\mathbf{b}$ in momentum space with $\tau = \pm 1$ the node index and chirality. The electronic dispersion in a small wave-vector region near each node is linear and isotropic. In a magnetic field $\mathbf{B} = B\hat{\mathbf{z}}$, this band structure is modified into a series of positive and negative energy Landau levels $n = \pm 1, \pm 2, \ldots$ which disperse along the direction of the magnetic field, and a chiral Landau level $n = 0$, with a linear dispersion given by $e_{\tau,n=0}(k_z) = -\tau\hbar v_F k_z$, where k_z is the component of the electron wave vector $\mathbf{k}$ along the direction of the magnetic field and v_F is the Fermi velocity. In the extreme quantum limit and for a small doping, the Fermi level is in the chiral levels near the Dirac point. It has been shown before that, when Coulomb interaction is considered, a Weyl semimetal may be unstable towards the formation of a condensate of internodal electron-hole pairs which gives rise in real space to an excitonic charge-density wave. This new state of matter is usually studied by using a short-range interaction between the electrons. In this paper we use the full long-range Coulomb interaction and the self-consistent Hartree-Fock approximation to generate the condensed state. We study its stability with respect to a change in the Fermi velocity, doping, and strength of the Coulomb interaction and also consider the situation where the Weyl nodes have a higher Chern number $C = 2, 3$ and more complex excitonic states are possible. We derive the response functions and collective excitations of the excitonic state working in the generalized random-phase approximation (GRPA). We show that, in the mean-field gap induced by the internodal coherence, there is, in the excitonic response function, a series of bound electron-hole states (excitons) with a binding energy that decreases until the renormalized Hartree-Fock energy gap is reached. In addition, there is a collective mode gapped at exactly the plasmon frequency. By contrast, the plasmon mode is the only excitation present in the density and current response functions. Despite the U(1) symmetry of the excitonic state, there is no gapless mode in the GRPA excitonic response. Indeed, the gapless mode present in the proper excitonic response function is pushed to the plasmon frequency by the long-range Coulomb interaction.

DOI: 10.1103/PhysRevB.110.035162

I. INTRODUCTION

The simplest model of a Weyl semimetal (WSM) with broken time-reversal symmetry consists of two Weyl nodes with opposite topological charges $C = \pm 1$ located in the Brillouin zone at the wave vectors $\mathbf{K}_\tau = \tau\mathbf{b}$, where $\tau = \pm 1$ is the node index. Near each node, the dispersion is linear and isotropic, i.e., $E_s = s\hbar v_F|\mathbf{k}|$, where the wave vector $\mathbf{k}$ is measured with respect to the Weyl points and $s = \pm 1$ is the band index [1]. In the presence of an external magnetic field $\mathbf{B}$ directed along the z axis, the band structure is transformed into a set of positive ($n > 1$) and negative ($n < 1$) Landau levels that disperse along the direction of the magnetic field according to $e_{\tau,n\neq 0}(k_z) = \frac{\hbar v_F}{\ell}\,\mathrm{sgn}(n)\sqrt{k_z^2\ell^2 + 2|n|}$, where k_z is the component of the wave vector $\mathbf{k}$ parallel to the magnetic field, v_F is the Fermi velocity, and $\ell = \sqrt{\hbar/eB}$ is the magnetic length. In addition, there is a single chiral $n = 0$ Landau level at each node that disperses linearly along the direction of the magnetic field according to $e_{\tau,n=0}(k_z) = -\tau\hbar v_F k_z$.

In the extreme quantum limit at zero temperature and in the absence of doping, the Fermi level is at the Dirac point in the chiral levels. It has been shown [2] that, in this situation, the internodal Coulomb exchange interaction can couple electrons and holes with different chiralities. This spontaneously hybridizes the two nodes of opposite chiralities and opens a gap in the chiral levels. The resulting state from this chiral symmetry breaking is an internodal condensate of electron-hole pairs that is characterized by a complex order parameter of the form $\langle\rho_{-,+}\rangle = (1/N_\varphi)\sum_{k_z,X}\langle c^\dagger_{k_z,X,-}c_{k_z,X,+}\rangle = |\langle\rho_{-,+}\rangle|e^{i\varphi}$, where X is the guiding-center index in the Landau gauge, $N_\varphi = S/2\pi\ell^2$ is the Landau-level degeneracy (with S the area of the WSM perpendicular to the magnetic field), the operators $c_{k_z,X,\tau}(c^\dagger_{k_z,X,\tau})$ destroy (create) an electron in state k_z, X, τ and $\langle\ldots\rangle$ denotes a ground-state average. These electron-hole pairs are loosely called excitons although they are not bound states but electrons and holes paired by the internodal exchange interaction and then condensed. The energy of this excitonic state is independent of the phase φ of its order parameter and so one would expect a Goldstone mode to be associated with this U(1) symmetry.

This excitonic state has been extensively studied in the literature (see, for example, Refs. [2–19]). In real space, the excitonic condensate leads to the formation of a charge-density wave (CDW) with density $\langle n(z)\rangle \sim |\langle\rho_{-,+}\rangle|\cos(2b_z z + \varphi)$ and so to nonlinear transport properties. The sliding motion of this incommensurate CDW (the phason), after depinning from the impurities, is the Goldstone mode associated with fluctuations in the phase φ. Fluctuations in the amplitude of

the order parameter are expected to be gapped. One important property of the excitonic CDW state is that its coupling with the electromagnetic field leads to an extra magnetoelectric axionic term in the action. The CDW is thus an example of an axionic state of matter [9] with the phason being an axion, a hypothetical particle first proposed in high-energy physics [20,21]. The formation of the excitonic condensate can occur with or without the presence of a magnetic field. Excitonic states with more complex order parameters are possible when $B = 0$ involving either internodal or intranodal electron-hole pairings.

In this paper, we study the spontaneous internodal excitonic state that can occur between the two chiral $n = 0$ Landau levels in the strong magnetic field limit where the Fermi level lies near the Dirac point and the upper Landau levels are empty. Contrary to most previous papers where the gap equation for the excitonic state is derived using a contact interaction, we use the full long-range Coulomb interaction. We solve the self-consistent Hartree-Fock equations for the single-particle Green's function numerically using an iterative method. We study how the internodal coherence $\langle\rho_{-,+}\rangle = \langle\rho_{+,-}\rangle^*$ depends on the Fermi velocity, Chern number $C = 1, 2, 3$, doping and strength of the Coulomb interaction using realistic values for these parameters. For higher Chern numbers $C = 2, 3$, there are, respectively, two and three degenerate chiral levels at each node and more complex excitonic states are possible involving internodal and/or interlevel coherences. We find that a change in the Fermi velocity v_F can produce a phase transition between two different excitonic states.

We also study the response functions and collective excitations in the excitonic state for the specific case of $C = 1$. We derive these responses in the generalized random-phase approximation (GRPA). As far as we know, this has not been made before for the excitonic phase of a WSM in the strong magnetic field limit. A similar calculation has been done for a Dirac semimetal [22] but the band structure was different and internodal coherence was not considered. For $C = 1$, one can define 16 basic response functions and the internodal coherence couples them all so that they have to be calculated numerically. From these 16 response functions, we obtain the density, current, and excitonic responses (they are defined in Sec. VI). Because of a cancellation between self-energy and vertex corrections, the only collective excitation in the current χ_{jj} and density χ_{nn} responses is the plasmon whose frequency is slightly modified, in the excitonic state, from its known value [23] $\omega_p(Q) = \sqrt{\frac{e^3 v_F B}{2\pi^2\varepsilon_0\hbar^2} + v_F^2 Q^2}$ in an incoherent (normal) state. Because of the linear dispersion of the chiral states, there is no continuum of electron-hole excitations in these two responses as it is transformed into the plasmon mode.

A more interesting function is the excitonic response χ_{exc} since it contains excitations related to the fluctuations in the amplitude and phase of the complex order parameter $\langle\rho_{-,+}\rangle$. When only the ladder diagrams are considered in the GRPA (i.e., the "proper" response), we find in χ_{exc} a series of electron-hole bound states (excitons) with binding energy $e_{B,n}$ where $n = 1, 2, 3, \ldots$. The energy of these resonances increases until a continuum of electron-hole scattering states is reached at an energy E_{conti}, which is the Hartree-Fock energy gap redshifted by the vertex corrections. The ladder diagrams in $\chi_{\text{exc}}(\omega, Q)$ and the coupling between the different response functions caused by the internodal coherence produce a gapless collective mode with frequency $\omega = v_F Q$. When the bubble diagrams (the long-range Coulomb interaction) are considered in the calculation, i.e., within the full GRPA, the binding energy of the excitonic states is only slightly modified but the gapless mode is transformed into the gapped plasmon mode present also in the density and current responses. There is no remaining gapless collective excitation in the GRPA collective mode spectrum of the excitonic state. Similar results are obtained when the GRPA is applied to the study of collective excitations in superconductors [24,25].

This paper is organized as follows: In Sec. II, we present the Hartree-Fock description of the excitonic phase for a WSM where only the chiral levels in each node are considered. Numerical results for this phase are given in Sec. III for Chern number $C = 1$ and in Sec. IV for $C = 2, 3$. The GRPA approach for the response functions in the coherent phase is described in Sec. V. We define the current, density, and excitonic response functions χ_{jj}, χ_{nn}, and χ_{exc} in Sec. VI. Exact analytical results are obtained for χ_{jj} and χ_{nn} but χ_{exc} has to be calculated numerically. Our numerical results for these response functions are presented in Secs. VII and VIII for the incoherent and coherent phases, respectively. We conclude in Sec. IX. The general Hartree-Fock formalism for Weyl nodes with an arbitrary number of Landau levels is described in Appendix A. The precise forms of the exchange interactions that intervene in the Hartree-Fock formalism for Chern numbers $C = 1, 2, 3$ are listed in Appendix B.

II. HARTREE-FOCK DESCRIPTION OF THE EXCITONIC PHASE

We consider a simple model of a Weyl semimetal (WSM) with broken time-reversal symmetry consisting of two nodes, with Chern number C, centered at wave vectors $\mathbf{b} = -\tau b\hat{\mathbf{z}}$ and with opposite chiralities $\tau = \pm 1$. The noninteracting Hamiltonian for each node, written in the basis of the two bands that cross, is given in the absence of a magnetic field by

$$h_\tau(\mathbf{k}) = \tau\hbar v_F \begin{pmatrix} k_z & \beta(k_x - ik_y)^C \\ \beta(k_x + ik_y)^C & -k_z \end{pmatrix}, \qquad (1)$$

where v_F is the Fermi velocity, $\mathbf{k}$ is a wave vector measured from the position of each Weyl node in momentum space, β is a material-dependent anisotropy factor, and $C = 1, 2, 3$ is the Chern number.

The derivation of the Landau levels in a magnetic field $\mathbf{B} = \nabla \times \mathbf{A} = B\hat{\mathbf{z}}$ and of the Hartree-Fock Hamiltonian and equation of motion for the single-particle Green's function is given in Appendix A. We present there the general case where an arbitrary number of Landau levels are kept and all types of coherence are considered (inter-Landau-level, internodal, and complete entanglement). In this section we adapt these results to the simplest case where only the C chiral levels in each node are kept in the Hilbert space. These levels are degenerate and have the dispersion

$$e_\tau(k) = -\tau\hbar v_F k_z. \qquad (2)$$

The corresponding eigenvectors are independent of τ and given by

$$w_{n,k_z,X}(\mathbf{r}_\perp, z) = \frac{1}{\sqrt{L_z}} e^{ik_z z} \begin{pmatrix} 0 \\ h_{n,X}(\mathbf{r}_\perp) \end{pmatrix}, \tag{3}$$

with the integer n taking the values $n = 0$ to $C-1$. In the Landau gauge, with the vector potential $\mathbf{A} = (0, Bx, 0)$, the wave functions of the two-dimensional electron gas are given by $h_{n,X}(\mathbf{r}_\perp) = \varphi_n(x - X)e^{-iXy/\ell^2}/\sqrt{L_y}$, where X is the guiding-center index and $\varphi_n(x)$ the wave functions of the one-dimensional harmonic oscillator. Each state (n, k_z, τ) has degeneracy $N_\varphi = S/2\pi\ell^2$, where $S = L_x L_y$ is the area of the WSM perpendicular to the magnetic field, $\ell = \sqrt{\hbar/eB}$ is the magnetic length, and $\mathbf{r}_\perp$ is a two-dimensional vector in the plane perpendicular to the magnetic field. The dimensions of the WSM are $L_x \times L_y \times L_z$. Since we keep only the chiral levels, we approximate the electron field operator by

$$\Psi_\tau(\mathbf{r}) \approx \sum_{n,k_z,X} w_{n,k_z,X}(\mathbf{r}_\perp) c_{n,k_z,X,\tau}, \tag{4}$$

where $c_{n,k_z,X,\tau}$ annihilates an electron in state (n, k_z, X, τ). To simplify the notation, we will write k instead of k_z hereafter.

For the many-body Hamiltonian of the electron gas, we take

$$\begin{aligned} H = &\sum_\tau \int d^3r\, \Psi_\tau^\dagger(\mathbf{r}) h_\tau(\mathbf{r}) \Psi_\tau(\mathbf{r}) \\ &+ \frac{1}{2} \sum_{\tau,\tau'} \int d^3r \int d^3r' \Psi_\tau^\dagger(\mathbf{r}) \Psi_{\tau'}^\dagger(\mathbf{r}') \\ &\times V(\mathbf{r} - \mathbf{r}') \Psi_{\tau'}(\mathbf{r}') \Psi_\tau(\mathbf{r}), \end{aligned} \tag{5}$$

where the long-range Coulomb interaction is given by (ε_r is the relative dielectric constant of the WSM)

$$V(\mathbf{r}) = \frac{1}{V} \sum_{\mathbf{q}} \frac{e^2}{\varepsilon_r \varepsilon_0 |q_\perp^2 + q_z^2|} e^{i\mathbf{q}_\perp \cdot \mathbf{r}_\perp} e^{iq_z z}. \tag{6}$$

We have kept in H only one combination of field operators that conserves the number of electrons at each node. A second but weaker combination is discussed in Appendix A.

To fully characterize a particular phase of the electron gas in the WSM, we use the set of ground-state averages $\{\langle \rho_{n,n'}^{(\tau,\tau')}(k) \rangle\}$ where the operators

$$\rho_{n,n'}^{(\tau,\tau')}(k) = \frac{1}{N_\varphi} \sum_X c_{n,k,X,\tau}^\dagger c_{n',k,X,\tau'}. \tag{7}$$

In terms of these operators, the Hartree-Fock Hamiltonian, for a phase that is not modulated spatially, is given by

$$\begin{aligned} H_{\rm HF} = &N_\varphi \sum_{n,k,\tau} e_\tau(k) \rho_{n,n}^{(\tau,\tau)}(k) \\ &- \frac{N_\varphi}{L_z} \sum_{\tau,\tau'} \sum_{k_1,k_2} \sum_{n_1,\ldots,n_4} X_{n_1,n_2,n_3,n_4}(k_2 - k_1) \\ &\times \left\langle \rho_{n_1,n_4}^{(\tau,\tau')}(k_1) \right\rangle \rho_{n_3,n_2}^{(\tau',\tau)}(k_2), \end{aligned} \tag{8}$$

where the Fock interactions $X_{n_1,n_2,n_3,n_4}(k)$ are defined in Eq. (A50). They are nonzero for $n_1 - n_2 + n_3 - n_4 = 0$ only so that there are 1, 6, and 19 nonzero interactions of which 1, 4, and 10 are different for $C = 1, 2, 3$, respectively. The Hartree term is absent from $H_{\rm HF}$ since it is canceled by the positive background of the WSM.

The diagonal components $\langle \rho_{n,n}^{(\tau,\tau)}(k) \rangle$ give the occupation $\nu \in [0, 1]$ of the state (n, k, τ). The operator $c_{nX,k,\tau}^\dagger c_{n'X,k,-\tau}$ creates an electron-hole pairing between the states n, X, k, τ and $n', X, k, -\tau$, so that a nonzero value of $\langle \rho_{n,n}^{(\tau,-\tau)}(k) \rangle$ signals a condensate of internodal electron-hole pairs in Landau level n, while $\langle \rho_{n,n'\neq n}^{(\tau,\tau)}(k) \rangle$ signals a condensate of inter-Landau-level electron hole pairs in node τ. The general case $\langle \rho_{n,n'}^{(\tau,-\tau)}(k) \rangle$ with $n \neq n'$ represents a full entanglement between the paired electron and hole. We loosely speak of these pairs as "excitons" although they are not bound states. We use the words excitonic state or coherent state to refer to the state where some type of coherence is nonzero. As we show below, such states are favored by the exchange part (the Fock pairing in $H_{\rm HF}$) of the Coulomb interaction.

We explain in the Appendix A how the $\langle \rho_{n,n'}^{(\tau,\tau')}(k) \rangle$'s are obtained by solving the equation of motion for the single-particle Matsubara Green's function

$$G_{n,n'}^{(\tau,\tau')}(k, \tau) = -\frac{1}{N_\phi} \sum_X \langle T_{\tau_0} c_{n,k,X,\tau}(\tau_0) c_{n',k,X,\tau'}^\dagger(0) \rangle, \tag{9}$$

where T_{τ_0} is the imaginary-time ordering operator and τ_0 in the parentheses is the imaginary time (not to be confused with the node index). When $\tau_0 = 0^-$, we have

$$\begin{aligned} \left\langle \rho_{n',n}^{(\tau',\tau)}(k) \right\rangle &= G_{n,n'}^{(\tau,\tau')}(k, \tau_0 = 0^-) \\ &= \frac{1}{\beta\hbar} \sum_{i\omega_n} e^{-i\omega_n 0^-} G_{n,n'}^{(\tau,\tau')}(k, i\omega_n), \end{aligned} \tag{10}$$

where the fermionic Matsubara frequencies ω_n are defined by $\omega_n = (2n+1)\pi/\beta\hbar$ with $n = 0, \pm 1, \pm 2, \ldots$ and where $\beta = 1/k_B T$ with T the temperature and k_B the Boltzmann constant.

The equation of motion is given by

$$\begin{aligned} &\left[i\omega_n - \frac{1}{\hbar}[e_\tau(k) - \mu] \right] G_{n,n'}^{(\tau,\tau')}(k, i\omega_n) \\ &\quad - \frac{1}{\hbar} \sum_{\tau'',n''} \Sigma_{n,n''}^{(\tau,\tau'')}(k) G_{n'',n'}^{(\tau'',\tau')}(k, i\omega_n) = \delta_{\tau,\tau'} \delta_{n,n'}, \end{aligned} \tag{11}$$

where the Fock self-energies are defined as

$$\Sigma_{n,n'}^{(\tau,\tau')}(k) = -\frac{1}{L_z} \sum_{k_1} \sum_{n_1,n_2} X_{n_1,n',n,n_2}(k - k_1) \left\langle \rho_{n_1,n_2}^{(\tau',\tau)}(k_1) \right\rangle \tag{12}$$

and μ is the chemical potential. Equation (11) is solved in the manner explained in the Appendix A. The ground-state energy per volume $E_{\rm HF}$ is then given by

$$\begin{aligned} E_{\rm HF} = &\frac{1}{2\pi\ell^2 L_z} \sum_{n,k,\tau} e_\tau(k) \left\langle \rho_{n,n}^{(\tau,\tau)}(k) \right\rangle \\ &- \frac{1}{4\pi\ell^2 L_z^2} \sum_{\tau,\tau'} \sum_{k_1,k_2} \sum_{n_1,\ldots,n_4} X_{n_1,n_2,n_3,n_4}(k_2 - k_1) \\ &\times \left\langle \rho_{n_1,n_4}^{(\tau,\tau')}(k_1) \right\rangle \left\langle \rho_{n_3,n_2}^{(\tau',\tau)}(k_2) \right\rangle. \end{aligned} \tag{13}$$

When $C = 1$, there are then only two states to consider: $(n = 0, \tau = +)$ and $(n = 0, \tau = -)$ and we can obtain some manageable analytical results. Dropping the $n = 0$ index, we write in this case the Green's function matrix as

$$G(k, i\omega_n) = \begin{pmatrix} G_{+,+}(k, i\omega_n) & G_{+,-}(k, i\omega_n) \\ G_{-,+}(k, i\omega_n) & G_{-,-}(k, i\omega_n) \end{pmatrix}. \tag{14}$$

It satisfies the equation of motion (in matrix form)

$$[I(i\hbar\omega_n + \mu) - F(k)]G(k, i\omega_n) = \hbar I_{2\times 2}, \tag{15}$$

where $I_{2\times 2}$ is the 2×2 unit matrix and the matrix $F(k)$ is defined by

$$F(k) = \begin{pmatrix} e_+(k) + \Sigma_{+,+}(k) & \Sigma_{+,-}(k) \\ \Sigma_{-,+}(k) & e_-(k) + \Sigma_{-,-}(k) \end{pmatrix}. \tag{16}$$

The self-energies are given by $(i, j = \pm)$

$$\Sigma_{i,j}(k) = -\frac{1}{L_z}\sum_{k_1} X(k - k_1)\langle\rho_{j,i}(k_1)\rangle \tag{17}$$

and the interaction

$$X(x) = X_{0,0,0,0}(x) = \frac{e^2}{2\pi\varepsilon_0\varepsilon_r}\frac{1}{2}\Gamma\left(0, \frac{x^2}{2}\right)e^{\frac{x^2}{2}}, \tag{18}$$

where $\Gamma(0, x)$ is the incomplete gamma function. To avoid the divergence at $x = k = 0$ of this interaction, we add a very small screening parameter η to the Coulomb interaction in Eq. (6), i.e., $y^2 \to y^2 + \eta^2$.

The Hermitian matrix $F(k)$ can be diagonalized for each value of k by solving the equation

$$F(k)U(k) = U(k)D(k), \tag{19}$$

where $U(k)$ is the matrix of the eigenvectors and $D(k)$ the diagonal matrix of the eigenvalues. The Green's function is then obtained from

$$G_{i,j}(k, i\omega_n) = \sum_{a=\pm}\frac{U_{i,a}(k)U^{\dagger}_{a,j}(k)}{i\omega_n - [E_a(k) - \mu]/\hbar} \tag{20}$$

and, at $T = 0$ K, the order parameters are given by

$$\langle\rho_{j,i}(k)\rangle = \sum_{a=\pm} U_{i,a}(k)U^{-1}_{a,j}(k)\Theta[e_F - E_a(k)], \tag{21}$$

where e_F is the Fermi level which can be positive (electron doping) or negative (hole doping) and $\Theta(x)$ is the Heaviside function. We consider that the doping, if present, is the same in both nodes. Equations (16)–(21) constitute a self-consistent system of equations that must be solved numerically.

The band structure in the coherent phase consists of two bands with dispersion

$$E_{\pm}(k) = \tfrac{1}{2}[\Sigma_+(k) + \Sigma_-(k)] \pm \tfrac{1}{2}\zeta(k), \tag{22}$$

where

$$\zeta(k) = \sqrt{[2e(k) - \Sigma_+(k) + \Sigma_-(k)]^2 + 4|\Sigma(k)|^2} \tag{23}$$

and

$$e(k) = \hbar v_F k. \tag{24}$$

The analytical expressions for the order parameters are, for each wave vector k,

$$\langle\rho_{\pm,\pm}\rangle = \mp\frac{1}{2\zeta}(\Sigma_+ - \Sigma_- - 2e \mp \zeta)\Theta(e_F - E_-) \pm \frac{1}{2\zeta}(\Sigma_+ - \Sigma_- - 2e \pm \zeta)\Theta(e_F - E_+), \tag{25}$$

$$\langle\rho_{-,+}\rangle = -\frac{\Sigma}{\zeta}[\Theta(e_F - E_-) - \Theta(e_F - E_+)] \tag{26}$$

and $\langle\rho_{+,-}(k)\rangle = \langle\rho_{-,+}(k)\rangle^*$. The following sum rules follow from the equation of motion:

$$|\langle\rho_{i,i}(k)\rangle|^2 + |\langle\rho_{i,-i}(k)\rangle|^2 = \langle\rho_{i,i}(k)\rangle \tag{27}$$

and

$$\sum_{j=\pm}\langle\rho_{j,j}(k)\rangle = \sum_j \Theta[e_F - E_j(k)]. \tag{28}$$

If we write the coherence factor as $\langle\rho_{+,-}(k_1)\rangle = |\langle\rho_{+,-}(k_1)\rangle|e^{i\varphi(k_1)}$, then the internode part of the Fock term in $E_{\rm HF}$ can be written as

$$-\frac{1}{4\pi\ell^2 L_z^2}\sum_{k_1,k_2} X(k_2 - k_1)|\langle\rho_{+,-}(k_1)\rangle| \times |\langle\rho_{-,+}(k_2)\rangle|\cos[\varphi(k_1) - \varphi(k_2)]. \tag{29}$$

The other terms in the Hartree-Fock energy do not depend on the choice of the phase $\varphi(k)$ and so it is clear that in the coherent state, the phase $\varphi(k)$ must be a constant independent of k to minimize the energy, i.e., the internodal excitonic ground state has a U(1) symmetry.

III. EXCITONIC STATE WITH $C = 1$

In our numerical calculation for $C = 1$, we choose a cutoff $k_c\ell = 15$ for the wave vector along the z direction so that the dimensionless wave vector $k\ell \in [-15, 15]$ in each node. We discretize this interval into $2N_p + 1$ points, taking $N_p = 1000$. We solve the self-consistent system of equations (25) and (26) using an iterative method. We find that very good convergence is obtained after only 100 iterations if we start the first iteration with the seed $\langle\rho_{\pm,\pm}(k)\rangle = \Theta(\pm k + k_F)$ and $\langle\rho_{+,-}(\pm k_F)\rangle = \langle\rho_{-,+}(\pm k_F)\rangle^* = 1$, where the Fermi wave vector $k_F\ell = 4\pi^2\ell^3 n_e$ is determined by the amount of doping, i.e., the density of added electrons n_e.

To allow coherence in the state $k = 0$ in the absence of doping, we remove $\frac{1}{2}$ electron at $k = 0$ in each node. In order for the excitonic phase to be the ground state, the cohesive energy $E_{\rm cohe} = E_{\rm HF} - E_N$ must be negative, where E_N is the energy of the normal phase (defined as the state with Coulomb interaction but without coherence). We study the effect of three parameters on the excitonic phase: the Fermi velocity v_F, the dielectric constant ε_r, and the doping level $k_F\ell$.

Figure 1 shows the band structure $E_{\pm}(k)$ in the coherent (blue lines) and incoherent (black lines) states in the absence of doping. We have removed a global energy shift $\Sigma_+(k) + \Sigma_-(k) = -\frac{1}{L_z}\sum_{k_1} X(k_1)$ [see Eq. (17)] in both curves to force them to coincide at $k = 0$. The dashed blue and black lines give the position of the Fermi level for the corresponding state. For this figure, $v_F/c = 0.001$ and $\varepsilon_r = 1$ (c is the speed

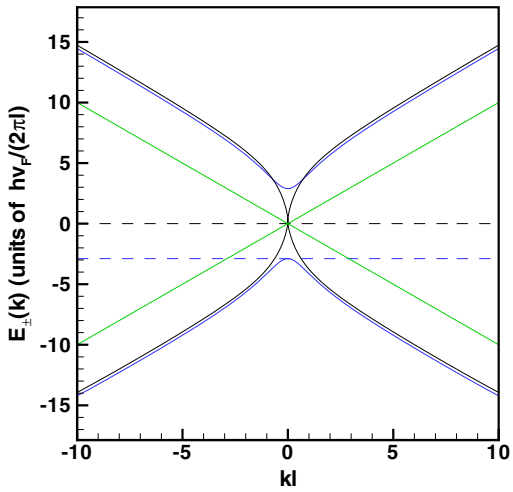

FIG. 1. Band structure in the undoped coherent and incoherent states. The blue (black) lines give the electronic dispersion $E_{\pm}(k)$ in the coherent (incoherent) states while the position of the Fermi level in each case is given by the dashed line of the corresponding color. A global energy shift has been removed in both cases to make all the curves centered at energy $E = 0$. The green lines show the noninteracting band structure. Parameters are $k_F\ell = 0$, $v_F/c = 0.001$, and $\varepsilon_r = 1$.

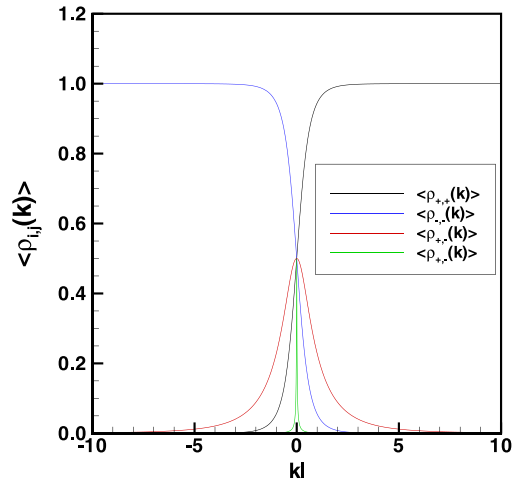

FIG. 2. Occupations and coherences $\langle\rho_{i,j}(k)\rangle$ in the undoped coherent phase. Parameters are $k_F\ell = 0$, $v_F/c = 0.001$, and $\varepsilon_r = 1$ with the exception of the green curve where $\varepsilon_r = 10$ and $v_F/c = 0.002$.

of light in vacuum). All energies are in units of $\hbar v_F/\ell = 7.69\sqrt{B}v_F/c$ eV. The noninteracting band structure (green lines) is modified by the self-energies $\Sigma_{\pm}(k)$ in both the coherent and incoherent states. The internodal coherence introduces a gap in the band structure. Since there is only one electron at $k\ell = 0$ in the undoped coherent state, the Fermi level is at the top of the bottom band and the system is insulating. In the original band structure, the two chiral levels would be separated by the wave vector $2\mathbf{b}$. However, since b does not enter our calculation, we are at liberty to set the origin of both levels at $k = 0$ in all the figures.

The corresponding occupations and coherences for the coherent state of Fig. 1 are shown in Fig. 2. They can be compared with the occupation of the k states in the incoherent state which is $\langle\rho_{\pm,\pm}(k)\rangle = \Theta(\mp k) = 1$ and $\langle\rho_{+,-}(k)\rangle = 0$. Internodal coherence leads to a modification of the occupation of the states near $k = 0$ where the coherence reaches its maximum value $\langle\rho_{+,-}(0)\rangle = \frac{1}{2}$ and, as required by the sum rules, $\langle\rho_{\pm,\pm}(0)\rangle = \frac{1}{2}$. As expected in a two-level system, the coherence decreases when the difference in the noninteracting energy $|e_+(k) - e_-(k)|$ increases and so it is maximal at $k = 0$ where the two noninteracting states are degenerate.

We use the integral $\langle\rho_{-,+}\rangle = \int dk\,\ell\langle\rho_{-,+}(k\ell)\rangle$ as an order parameter for the internodal excitonic state. The phase of $\langle\rho_{-,+}(k\ell)\rangle$ being arbitrary, $\langle\rho_{-,+}\rangle$ can be chosen real without any loss of generality. Figure 3 shows how this quantity depends on the Fermi velocity v_F/c and relative dielectric constant ε_r. Clearly, the coherence decreases rapidly when either one of these parameters is increased. Indeed, an increase in ε_r decreases the strength of the Coulomb interaction and an increase in v_F increases the separation in energy of the two levels at k thus decreasing the coherence. When v_F or ε_r increases, $E_{\text{cohe}} \to 0$ and $\langle\rho_{-,+}\rangle \to 0$.

We now consider the effect of doping which can be controlled by electric gating in a WSM. For a single chiral level, the density of states is a constant given by $g(\varepsilon) = 1/4\pi^2\ell^2\hbar v_F$ so that the Fermi wave vector k_F is related to the density of added electrons per node by $k_F\ell = 4\pi^2\ell^3 n_e$. For $k_F\ell = 0.25$, the electronic density is $n_e = 3.75 \times 10^{20} B^{\frac{3}{2}}$ e/m^3, a value that is not atypical in WSMs.

Figure 4 shows the band structure for $k_F\ell = 0.2$ with $v_F/c = 0.001$ and $\varepsilon_r = 1$. The Fermi level is indicated by the dashed line. The energy gap at $k = 0$ is still present, but the system is now metallic. The corresponding occupations and coherences are plotted in Fig. 5. No coherence is possible when a k state is fully occupied in both nodes so that the occupations are modified only near $\pm k_F\ell$ and coherence occurs only for $|k\ell| > k_F\ell$.

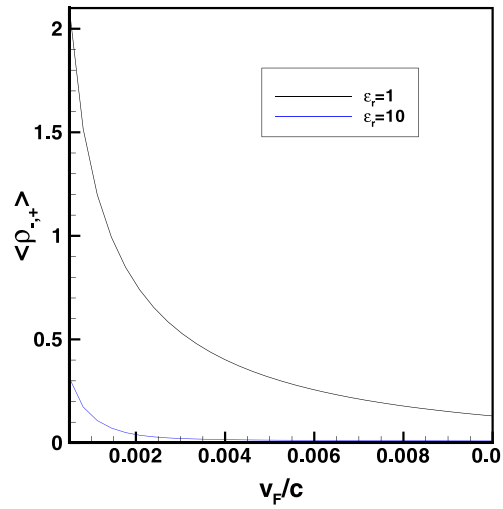

FIG. 3. Behavior of the order parameter $\langle\rho_{-,+}\rangle$ with the Fermi velocity in the undoped coherent phase for two different values of the dielectric constants: $\varepsilon_r = 1, 10$.

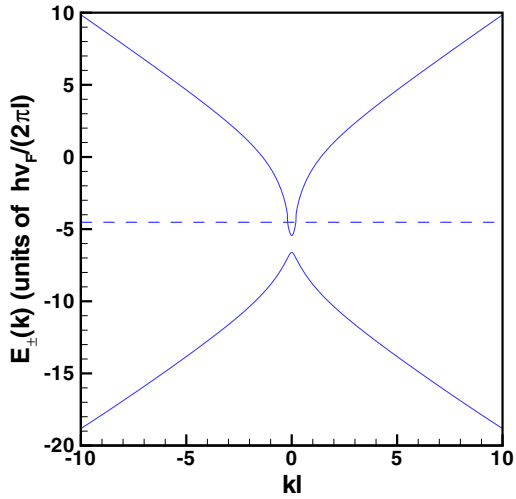

FIG. 4. Band structure of the doped coherent state. Parameters are $k_F\ell = 0.2$, $v_F/c = 0.001$, and $\varepsilon_r = 1$. The position of the Fermi level is indicated by the dashed line.

Figure 6 shows how the order parameter $\langle\rho_{-,+}\rangle$ depends on the doping level. An increase in $k_F\ell$ means that coherence has to be established between two noninteracting levels with higher energy separation and is consequently weaker. By electron-hole symmetry of the original band structure, the same results are obtained for hole doping.

The results of this section show that the excitonic state can be realized with realistic values of the Fermi velocity, dielectric constant, and doping. However, it is fragile and disappears rapidly as these parameters are increased.

At this point, we must say a word about the validity of our approximations. In order to restrict the Hilbert space to the chiral levels, we need the Coulomb interaction to be small with respect to the energy gap between the $n = 0$ and ± 1 Landau levels of the noninteracting electron gas. That is, we must ensure that $e^2/4\pi\varepsilon_0\varepsilon_r\ell < \sqrt{2}\hbar v_F/\ell$, i.e., $\alpha/\varepsilon_r\overline{v}_F \ll \sqrt{2}$, where $\alpha = e^2/4\pi\varepsilon_0\hbar c$ is the fine-structure constant and $\overline{v}_F = v_F/c$. Since ε_r can be large in a WSM, this condition can

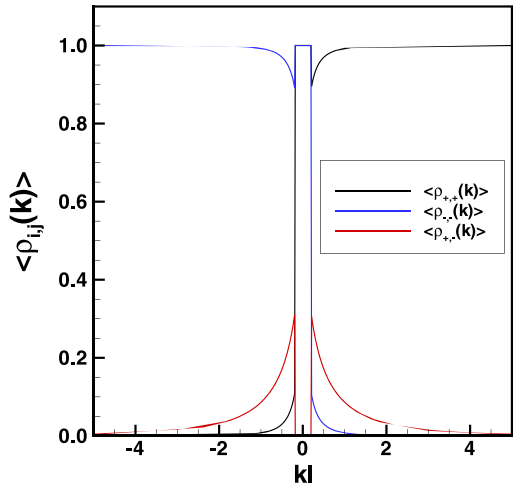

FIG. 5. Occupations and coherences $\langle\rho_{i,j}(k)\rangle$ in the doped coherent state. Parameters are $k_F\ell = 0.2$, $v_F/c = 0.001$, and $\varepsilon_r = 1$.

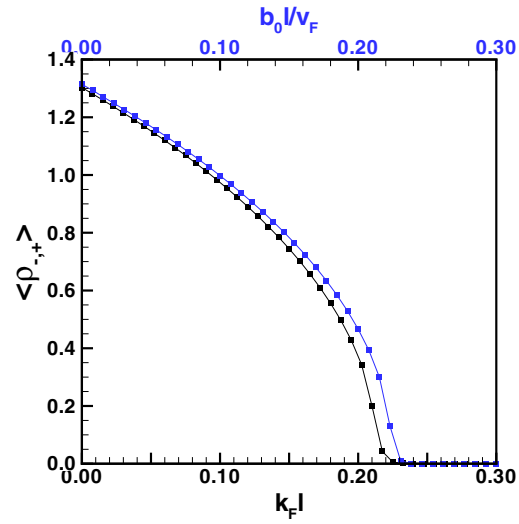

FIG. 6. Behavior of the order parameter $\langle\rho_{-,+}\rangle$ with electronic doping $k_F\ell$ in the coherent phase (bottom axis) and with the bias b_0 (top axis). Parameters are $v_F/c = 0.001$ and $\varepsilon_r = 1$.

be satisfied in principle. However, as our calculation shows, the coherence $\langle\rho_{-,+}\rangle$ decreases rapidly with the product $\varepsilon_r\overline{v}_F$. Nevertheless, Fig. 3 shows that there are a range of values of $\varepsilon_r\overline{v}_F$ where this condition is satisfied and coherence is possible.

The calculation of the self-energy implies integration over the wave vector k and so we must ensure that the cutoff wave vector k_c is such that the energy in the chiral band is lower than that of the $n = 1$ Landau level which implies $k_c\ell < \sqrt{2}$. This requires that the modification of the occupations from their noninteracting value be negligible for $k\ell > \sqrt{2}$. As Fig. 2 shows, this is not the case for $\varepsilon_r = 1$ and $\overline{v}_F = 0.001$ but the condition is satisfied for $\varepsilon_r = 10$ and $\overline{v}_F = 0.002$ (the green curve).

When doping is considered, the Fermi level must also be below the $n = 1$ Landau band. This condition is satisfied in our numerical calculation since, as shown in Fig. 6, the coherence $\langle\rho_{-,+}\rangle$ decreases to zero well before $k_F\ell = \sqrt{2}$ is reached.

Our calculation assumes $T = 0$ K. In the absence of doping and for the set of parameters $v_F/c = 0.001$, $\varepsilon_r = 1$, and $B = 10$ T, the difference in the energy per electron between the coherent and incoherent states (the cohesive energy) is approximately 4 K while for $v_F/c = 0.002$, $\varepsilon_r = 10$, and $B = 10$ T, where the coherence is much smaller (see Fig. 3), this difference decreases to 4 mK. If we use these figures to approximate the melting temperature for the coherent state, then we can conclude that the coherence should survive at finite, but small, temperature.

Although the discovery of a WSM with a single pair of Weyl nodes, $Eu_3In_2As_4$, has been reported recently [26] (and others should exist according to *ab initio* calculations), most WSMs have more than two Weyl points. Because the internodal coherence occurs in momentum space and not in real space, we believe that it should remain possible in WSMs with more pairs of nodes. That is, if their Dirac points are at the same energy. If they are not, then the doping of the different

nodes will be different and the coherence will probably be lost. To verify this, we calculated the effect of adding an electrical bias that shifts the energy of the two nodes. In our model, this is done by adding the term $-\tau\hbar b_0$ to the single-particle energy in Eq. (2) and the term $\hbar b_0$ to $e(k)$ in Eq. (24). In the incoherent state, $\langle\rho_{+,+}(k)\rangle = 1$ for $k\ell \in [-2\frac{b_0\ell}{v_F}, k_c\ell]$ and $\langle\rho_{-,-}(k)\rangle = 1$ for $k\ell \in [-k_c\ell, 0]$ so that there is a difference in density of added electrons given by $\Delta n_e = b_0/2\pi^2 v_F\ell^2$ between the two nodes. Coherence cannot be established in the region $k\ell \in [-2\frac{b_0\ell}{v_F}, 0]$ where the two chiral levels are occupied. It can only occur in the flanks of this region which is indeed what we find numerically. The blue line in Fig. 6 shows how the order parameter decreases with b_0. As expected, the coherence decreases with the electrical bias. For $B = 10$ T and $v_F/c = 0.001$, it vanishes for $\hbar b_0 \gtrsim 6.3$ meV. Note that we assume that the two nodes are at equilibrium so that they share the same Fermi level.

In concluding this section, we remark that the excitonic state in our description is uniform spatially since we consider the two nodes as separate systems and write the total density as $n(\mathbf{r}, z) = \sum_\tau \Psi^\dagger_\tau(\mathbf{r}, z)\Psi_\tau(\mathbf{r}, z)$. But, when the two nodes are considered as one system, the density should be written as $n(\mathbf{r}, z) = \Psi^\dagger(\mathbf{r}, z)\Psi(\mathbf{r}, z)$ with the field operator defined by

$$\Psi(\mathbf{r}, z) = w_{0,k,X}(\mathbf{r}_\perp, z)e^{-ibz}c_{k,X,-} + w_{0,k,X}(\mathbf{r}_\perp, z)e^{ibz}c_{k,X,+}, \tag{30}$$

where the summation over k is restricted to the small-momentum region near each node where the dispersion is linear. Performing an integration over $\mathbf{r}_\perp$, we have for the average density along the z direction apart from an unimportant constant

$$\langle n(z)\rangle \sim \frac{S}{2\pi^2\ell^3}\cos(2bz + \varphi)\langle\rho_{-,+}\rangle, \tag{31}$$

where φ is the U(1) phase of the complex order parameter $\langle\rho_{-,+}\rangle$. In this description, the excitonic phase is also a charge-density wave state which is modulated by the axion wave vector b and whose amplitude depends on the magnetic field and order parameter.

IV. EXCITONIC STATES FOR CHERN NUMBERS $C = 2$ AND 3

For Weyl nodes with Chern number $C = 2, 3$, there are, respectively, 4 and 6 quantum states to consider. We denote them by the superindices $I, J = (n, \tau) = 1, 2, \ldots, 6$ with the correspondence

$$\begin{aligned} &1 = (0, +); 2 = (0, -),\\ &3 = (1, +); 4 = (1, -),\\ &5 = (2, +); 6 = (2, -). \end{aligned} \tag{32}$$

We solve the equation of motion for the Green's function given in Eq. (A37). The components of the F matrix are defined by

$$F_{I,J}(k) = \frac{1}{\hbar}[(-\tau\hbar v_F k - \mu)\delta_{I,J} - \Sigma_{I,J}(k)], \tag{33}$$

where the self-energies for $C = 1, 2$ are given by

$$\Sigma^{(\tau,\tau')}_{n,n}(k) = -\frac{1}{L_z}\sum_{k_1}\sum_{n_1} X_{n_1,n,n,n_1}(k - k_1)\langle\rho^{(\tau,\tau')}_{n_1,n_1}(k_1)\rangle \tag{34}$$

and

$$\Sigma^{(\tau,\tau')}_{n,n'\neq n}(k) = -\frac{1}{L_z}\sum_{k_1} X_{n',n',n,n}(k - k_1)\langle\rho^{(\tau',\tau)}_{n',n}(k_1)\rangle. \tag{35}$$

For $C = 3$, however, there are four additional contributions to some of the self-energies $\Sigma^{(\tau,\tau')}_{n,n'\neq n}(k)$ which are given by

$$\Sigma^{(\tau,\tau')}_{0,1}(k) \to -\frac{1}{L_z}\sum_{k_1} X_{2,1,0,1}(k - k_1)\langle\rho^{(\tau',\tau)}_{2,1}(k_1)\rangle, \tag{36}$$

$$\Sigma^{(\tau,\tau')}_{1,0}(k) \to -\frac{1}{L_z}\sum_{k_1} X_{1,0,1,2}(k - k_1)\langle\rho^{(\tau',\tau)}_{1,2}(k_1)\rangle \tag{37}$$

and

$$\Sigma^{(\tau,\tau')}_{1,2}(k) \to -\frac{1}{L_z}\sum_{k_1} X_{1,2,1,0}(k - k_1)\langle\rho^{(\tau',\tau)}_{1,0}(k_1)\rangle, \tag{38}$$

$$\Sigma^{(\tau,\tau')}_{2,1}(k) \to -\frac{1}{L_z}\sum_{k_1} X_{0,1,2,1}(k - k_1)\langle\rho^{(\tau',\tau)}_{0,1}(k_1)\rangle. \tag{39}$$

Figure 7(a) shows the occupations and coherences and Fig. 7(b) the corresponding band structure for $C = 2$ in the excitonic state for $v_F/c = 0.001$ and $\varepsilon_r = 1$. The band structure in the absence of coherence but with interaction is shown in the inset of Fig. 7(b) for $C = 2$. The $n = 0, 1$ bands have different self-energies. They are thus shifted differently in energy creating many degeneracy points. As with $C = 1$, the coherences gap the whole band structure. For Fermi velocity $v_F/c \in [0.001, 0.1]$, only internodal coherence in the same band is present. It decreases with v_F/c as shown in the inset of Fig. 7(d) and, at $v_F/c \approx 0.011$, it drops abruptly to zero where it is replaced by entanglement between states (1, 4) and (2, 3) as shown in Fig. 7(c). The corresponding band structure after this phase transition is shown in Fig. 7(d). It is modified from the interacting but incoherent band structure shown in the inset of Fig. 7(b) but only in a very small range of wave vector $k\ell$.

Figure 8(a) shows the occupations and coherences and Fig. 8(b) the corresponding band structure for $C = 3$ in the excitonic state for $v_F/c = 0.001$ and $\varepsilon_r = 1$. As for $C = 2$, only internodal coherence in the same band is present at this Fermi velocity and the band structure is gapped. We find that this ground state persists up to $v_F/c \approx 0.006$ where there is a transition to a different type of coherent state that we were not able to identify completely, the number of such states being quite large for $C = 3$.

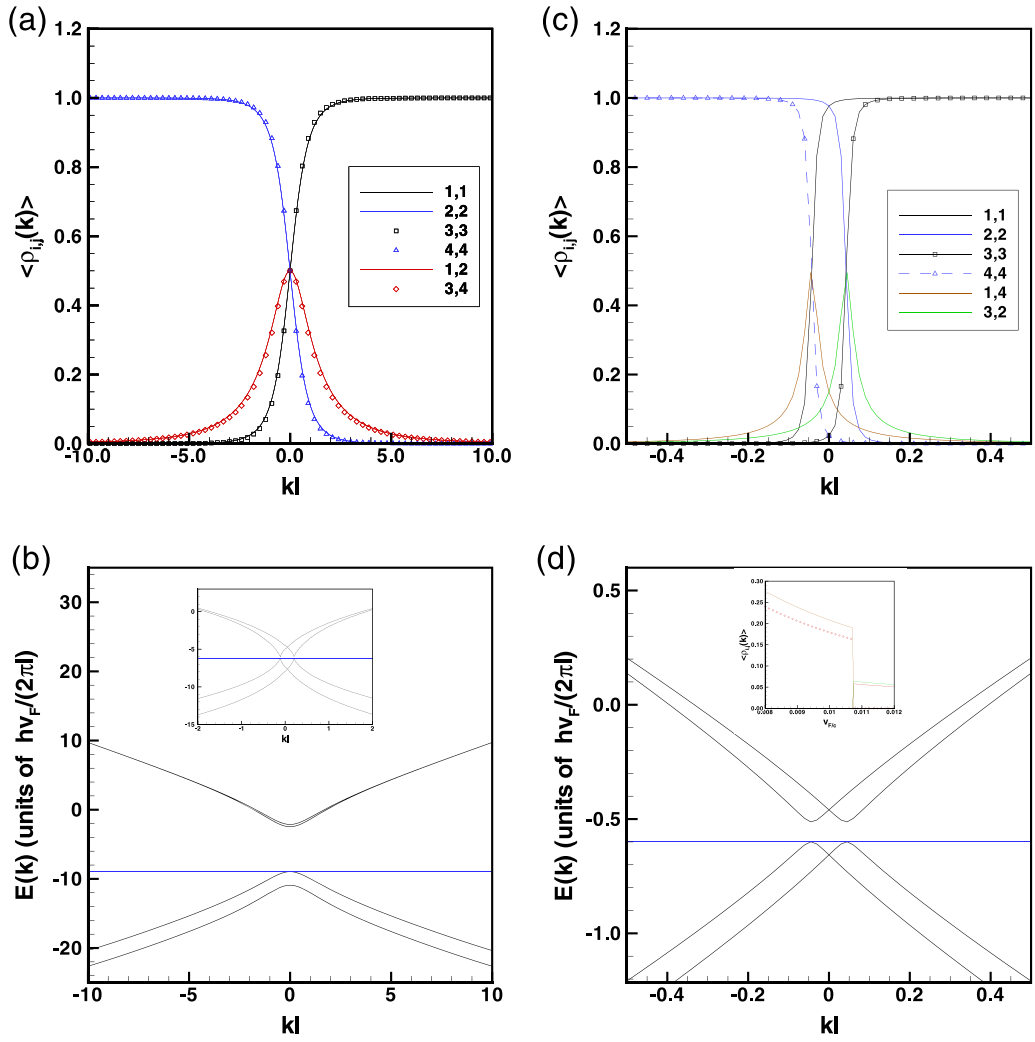

FIG. 7. Excitonic state for $C = 2$. (a) Occupations and coherences and (b) band structure for $v_F/c = 0.001$. (c), (d) Show the same but for $v_F/c = 0.01$. The inset in (b) shows the gapless band structure in the absence of coherence and that in (d) shows the behavior of the coherences with v_F/c [the lines legend is as in (c)]. The blue lines in (b) and (d) indicate the position of the Fermi level. Parameters are $k_F\ell = 0$ and $\varepsilon_r = 1$.

When only internodal coherence in the same level is present, the ground-state energy per volume V is given by

$$\frac{E_{\rm HF}}{V} = \frac{1}{2\pi\ell^2}\frac{1}{L_z}\sum_{n,k,\tau} e_\tau(k)\langle\rho^{(\tau,\tau)}_{n,n}(k)\rangle - \frac{1}{2\pi\ell^2}\frac{1}{L_z^2}\sum_{\tau}\sum_{k_1,k_2}\sum_{n_1,n_2} X_{n_1,n_2,n_2,n_1}(k_2-k_1)\langle\rho^{(\tau,\tau)}_{n_1,n_1}(k_1)\rangle\langle\rho^{(\tau,\tau)}_{n_2,n_2}(k_2)\rangle$$

$$- \frac{2}{2\pi\ell^2}\frac{1}{L_z^2}\sum_{k_1,k_2}\sum_{n_1} X_{n_1,n_1,n_1,n_1}(k_2-k_1)|\langle\rho^{(+,-)}_{n_1,n_1}(k_1)\rangle||\langle\rho^{(-,+)}_{n_1,n_1}(k_2)\rangle|\cos[\varphi_{n_1}(k_1)-\varphi_{n_1}(k_2)]$$

$$- \frac{2}{2\pi\ell^2}\frac{1}{L_z^2}\sum_{k_1,k_2}\sum_{n_1,n_2\neq n_1} X_{n_1,n_2,n_2,n_1}(k_2-k_1)|\langle\rho^{(+,-)}_{n_1,n_1}(k_1)\rangle||\langle\rho^{(-,+)}_{n_2,n_2}(k_2)\rangle|\cos[\varphi_{n_1}(k_1)-\varphi_{n_2}(k_2)], \quad (40)$$

with the phases defined by $\langle\rho^{(+,-)}_{n,n}(k)\rangle = |\langle\rho^{(+,-)}_{n,n}(k)\rangle|e^{i\varphi_n(k)}$. The energy is minimized when $\varphi_{n_1}(k_1) = \varphi_{n_1}(k_2)$ and $\varphi_{n_1}(k_1) = \varphi_{n_2}(k_2)$. Thus, all internodal coherent states for $C = 1, 2, 3$ are invariant with respect to one global phase.

V. GENERAL EQUATION FOR THE RESPONSE FUNCTIONS

In order to derive the response functions in the excitonic state we compute the two-particle Matsubara Green's

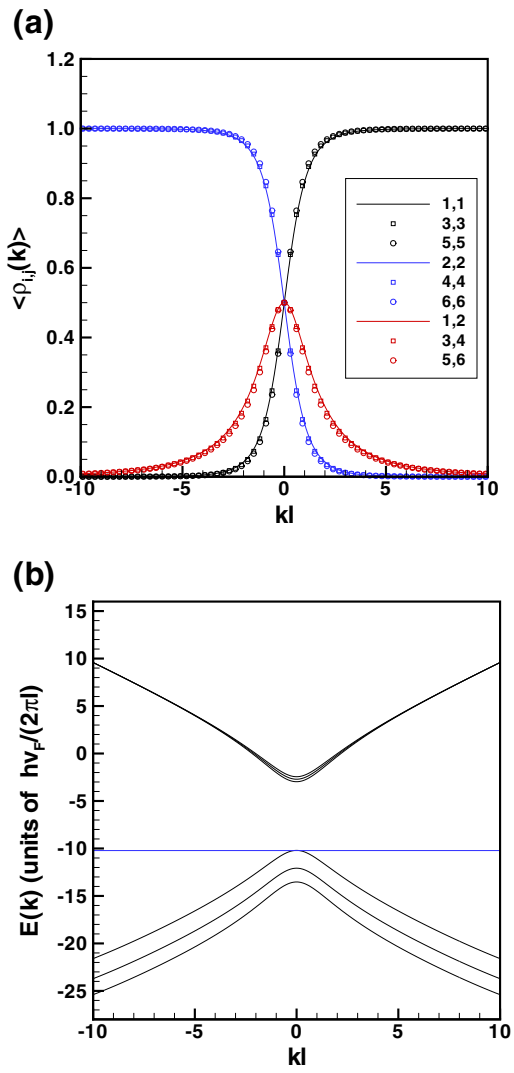

FIG. 8. Excitonic state for $C = 3$. (a) Occupations and coherences and (b) band structure. The blue line in (b) indicates the position of the Fermi level. Parameters are $v_F/c = 0.001$, $k_F\ell = 0$, and $\varepsilon_r = 1$.

functions

$$L_{a,b,c,d}(1,2,3,4) = -\langle T\Psi_a^\dagger(1)\Psi_b(2)\Psi_c^\dagger(3)\Psi_d(4)\rangle + G_{b,a}(2,1)G_{d,c}(4,3), \tag{41}$$

where the single-particle Matsubara Green's function is defined by

$$G_{a,b}(1,2) = -\langle T\Psi_a(1)\Psi_b^\dagger(2)\rangle. \tag{42}$$

The numbers refer to the position vector and imaginary time, i.e., $1 = (\mathbf{u}_1, \tau_1)$, the integral $\int d\bar{1} = \int_0^{\beta\hbar} d\tau_1 \int d^3r_1$ and a, b, c, d are node indices.

The single-particle Green's function introduced in the previous section was computed in the Hartree-Fock approximation which is defined by

$$G_{a,b}(1,2) = G^0_{a,b}(1,2) + \sum_{c,d}\int d\bar{3}\, G^0_{a,c}(1,\bar{3})\Sigma^{\rm HF}_{c,d}(\bar{3},\bar{4}) \times G_{d,b}(\bar{4},2), \tag{43}$$

where $G^0_{a,c}$ is a noninteracting Green's function and the Hartree-Fock self-energy is defined by

$$\Sigma_{c,d}(5,6) = \frac{1}{\hbar}\delta_{c,d}\int d\bar{7}\,\delta(5-6)V(5-\bar{7})G_{g,g}(\bar{7},\bar{7}^+) - \frac{1}{\hbar}V(5-6)G_{c,d}(5,6), \tag{44}$$

where $V(1-2) = V(\mathbf{u}_1 - \mathbf{u}_2)\delta(\tau_1 - \tau_2)$ is the Coulomb interaction which is independent of the node index. The two terms on the right-hand side of Eq. (44) are, respectively, the Hartree and Fock self-energies.

We derive the two-particle Green's function in the generalized random-phase approximation (GRPA) which consists in the summation of bubble and ladder diagrams. The GRPA is obtained by a functional derivative of the single-particle Green's function and is a conserving approximation [27]. More precisely, it is defined by the equation

$$L_{a,b,c,d}(1,2,3,4) = G_{b,c}(2,3)G_{d,a}(4,1) + \sum_{e,g}\frac{1}{\hbar}\int d\bar{5}\int d\bar{6}\, G_{b,e}(2,\bar{5})G_{e,a}(\bar{5},1)V(\bar{5}-\bar{6})L_{g,g,c,d}(\overline{6^+},\bar{6},3,4) - \sum_{e,f}\frac{1}{\hbar}\int d\bar{5}\int d\bar{6}\, G_{b,e}(2,\bar{5})G_{f,a}(\bar{6},1)V(\bar{5}-\bar{6})L_{f,e,c,d}(\bar{6},\bar{5},3,4). \tag{45}$$

This equation couples all 16 Green's functions together and we can extract from it the two-particle Green's functions

$$P^{\tau_a,\tau_b,\tau_c,\tau_d}_{k_1,k_2,k_3,k_4}(\mathbf{q}_\perp,\mathbf{q}'_\perp;\tau) = -N_\varphi\langle T\rho_{\tau_a,\tau_b}(\mathbf{q}_\perp,k_1,k_2;\tau)\rho_{\tau_c,\tau_d}(-\mathbf{q}'_\perp,k_3,k_4;0)\rangle, \tag{46}$$

where the operators $\rho_{\tau_a,\tau_b}(\mathbf{q}_\perp,k,k';\tau)$ now depend on imaginary time and are defined by

$$\rho_{\tau_a,\tau_b}(\mathbf{q}_\perp,k,k';\tau) = \frac{1}{N_\varphi}\sum_X e^{-iq_xX}e^{iq_xq_y\ell^2/2}c^\dagger_{k,X,\tau_a}(\tau)c_{k',X-q_y\ell^2,\tau_b}(\tau). \tag{47}$$

We calculate the two-particle Green's function in the uniform state so that only the occupation and coherences $\langle\rho_{\tau_a,\tau_b}(\mathbf{q}_\perp = 0,k,k)\rangle = \langle\rho^{\tau_a,\tau_b}(k)\rangle$ are nonzero. Moreover, we restrict our analysis to response functions with wave vectors

along the direction of the magnetic field, i.e., take $\mathbf{q}_\perp = \mathbf{q}'_\perp = 0$ in $P^{\tau_a,\tau_b,\tau_c,\tau_d}_{k_1,k_2,k_3,k_4}(\mathbf{q}_\perp, \mathbf{q}'_\perp; \tau)$.

One of us (R.C.) has given in Appendix A of Ref. [28] a detailed derivation of the GRPA equation of motion for $L_{a,b,c,d}(1,2,3,4)$ and $P^{\tau_a,\tau_b,\tau_c,\tau_d}_{k_1,k_2,k_3,k_4}(0,0;i\Omega_n)$, where $\Omega_n = 2n\pi/\beta\hbar$ with $n = 0, \pm1, \pm2, \ldots$ is a bosonic Matsubara frequency. We refer the reader to this Appendix and give here only the main results.

Hereafter, we restrict our analysis to nodes with Chern number $C = 1$ in order for the size of the matrices that are involved in the calculation to be manageable numerically. We first define a matrix containing the 16 response functions

$$P^{I,J}_{k+Q,k}(\omega) = \sum_{k'} P^{I,J}_{k+Q,k,k',k'+Q}(\omega), \tag{48}$$

where the superindices $I, J = 1, 2, 3, 4$ are defined in the following way: for the rows $I = (\tau_a, \tau_b) = (+,+), (+,-), (-,+), (-,-)$ and, for the columns $J = (\tau_c, \tau_d) = (+,+), (-,+), (+,-), (-,-)$. We also define the matrices

$$\overline{E}(k,Q) = \frac{1}{\hbar}\begin{pmatrix} [e_+(k) - e_+(k+Q)] & 0 & 0 & 0 \\ 0 & e_-(k) - e_+(k+Q) & 0 & 0 \\ 0 & 0 & e_+(k) - e_-(k+Q) & 0 \\ 0 & 0 & 0 & e_-(k) - e_-(k+Q) \end{pmatrix} \tag{49}$$

and

$$\overline{\Sigma}(k,Q) = \frac{1}{\hbar}\begin{pmatrix} [\Sigma_+(k) - \Sigma_+(k+Q)] & \Sigma(k) & -\Sigma(k+Q) & 0 \\ \Sigma(k) & \Sigma_-(k) - \Sigma(k+Q) & 0 & -\Sigma(k+Q) \\ -\Sigma(k+Q) & 0 & \Sigma_+(k) - \Sigma_-(k+Q) & \Sigma(k) \\ 0 & -\Sigma(k+Q) & \Sigma(k) & \Sigma_-(k) - \Sigma_-(k+Q) \end{pmatrix} \tag{50}$$

and

$$\overline{B}(k,Q) = \begin{pmatrix} \langle\rho_{+,+}(k+Q)\rangle - \langle\rho_{+,+}(k)\rangle & -\langle\rho_{-,+}(k)\rangle & \langle\rho_{+,-}(k+Q)\rangle & 0 \\ -\langle\rho_{+,-}(k)\rangle & \langle\rho_{+,+}(k+Q)\rangle - \langle\rho_{-,-}(k)\rangle & 0 & \langle\rho_{+,-}(k+Q)\rangle \\ \langle\rho_{-,+}(k+Q)\rangle & 0 & \langle\rho_{-,-}(k+Q)\rangle - \langle\rho_{+,+}(k)\rangle & -\langle\rho_{-,+}(k)\rangle \\ 0 & \langle\rho_{-,+}(k+Q)\rangle & -\langle\rho_{+,-}(k)\rangle & \langle\rho_{-,-}(k+Q)\rangle - \langle\rho_{-,-}(k)\rangle \end{pmatrix} \tag{51}$$

and these other matrices

$$\overline{H}(Q) = \frac{e^2}{\varepsilon_0\hbar}\begin{pmatrix} H(Q) & 0 & 0 & H(Q) \\ 0 & 0 & 0 & 0 \\ 0 & 0 & 0 & 0 \\ H(Q) & 0 & 0 & H(Q) \end{pmatrix} \tag{52}$$

and

$$\overline{X}(k) = \frac{e^2}{\varepsilon_0\hbar}\begin{pmatrix} X(k) & 0 & 0 & 0 \\ 0 & X(k) & 0 & 0 \\ 0 & 0 & X(k) & 0 \\ 0 & 0 & 0 & X(k) \end{pmatrix}, \tag{53}$$

where

$$H(Q) = \frac{1}{2\pi}\frac{1}{(Q\ell)^2}, \tag{54}$$

$$X(k) = \frac{1}{4\pi}e^{\frac{(k\ell)^2}{2}}\Gamma\left(0, \frac{(k\ell)^2}{2}\right). \tag{55}$$

We can then write the GRPA system of equations for the response function in the compact matrix form

$$\begin{aligned}[I(i\Omega_n) - \overline{E}(k,Q) - \overline{\Sigma}(k,Q)]\overline{P}_{k+Q,k}(i\Omega_n) &= \overline{B}(k,Q) + \overline{B}(k,Q)\overline{H}(Q)\frac{1}{L_z}\sum_{k'}\overline{P}_{k'+Q,k'}(i\Omega_n) \\ &\quad - \frac{1}{L_z}\sum_{k'}\overline{B}(k,Q)\overline{X}(k-k')\overline{P}_{k'+Q,k'}(i\Omega_n).\end{aligned} \tag{56}$$

Once all the elements of the matrix $\overline{P}_{k+Q,k}(\omega)$ have been calculated, we obtain the retarded responses by making the analytic continuation $i\Omega_n \to \omega + i\delta$ and then summing over k, i.e.,

$$\overline{P}(\omega,Q) = \frac{N_\varphi}{SL_z}\sum_k \overline{P}_{k+Q,k}(\omega). \tag{57}$$

We also use below the proper response functions $\widetilde{\overline{P}}_{k+Q,k}(i\Omega_n)$, which are defined by the summation of the connected diagrams only, i.e., by setting $\overline{H}(Q)$ in Eq. (56)

so that

$$\frac{1}{L_z}\sum_{k'}[(I(i\Omega_n)-\overline{E}(k,Q)-\overline{\Sigma}(k,Q))L_z\delta_{k,k'} + \overline{B}(k,Q)\overline{X}(k-k')]\overline{\overline{P}}_{k'+Q,k'}(i\Omega_n)=\overline{B}(k,Q). \quad (58)$$

In terms of the proper response functions, the GRPA equation can be written as

$$\overline{P}_{k+Q,k}(i\Omega_n)=\overline{\overline{P}}_{k+Q,k}(i\Omega_n)+\overline{\overline{P}}_{k+Q,k}(i\Omega_n)\overline{H}(Q) \times\frac{1}{L_z}\sum_{k'}\overline{P}_{k'+Q,k'}(\omega). \quad (59)$$

VI. DENSITY, CURRENT, AND EXCITONIC RESPONSE FUNCTIONS

In this section, we define the density, current, and excitonic response functions. The Fourier transform $n(\mathbf{q}_\perp, q_z)$ of the second-quantized charge-density operator is given by

$$n(0,Q)=-e\sum_\tau\int d\mathbf{u}\,\Psi^\dagger_\tau(\mathbf{u})e^{-iQz}\Psi_\tau(\mathbf{u}) =-eN_\varphi\sum_{\tau,k}\rho_{\tau,\tau}(\mathbf{q}_\perp=0,k,k+Q), \quad (60)$$

while, with the current operator given by $j_{z,\tau}=-e\tau v_F\sigma_z$, the second-quantized form $J_{z,\tau}(\mathbf{q}_\perp, q_z)$ is

$$J_{z,\tau}(0,Q)=\int d\mathbf{u}\,\Psi^\dagger_\tau(\mathbf{u})e^{-iQz}j_{z,\tau}\Psi_\tau(\mathbf{u}) =ev_FN_\varphi\sum_{\tau,k}\tau\rho_{\tau,\tau}(\mathbf{q}_\perp=0,k,k+Q). \quad (61)$$

Thus, the density χ_{nn} and current χ_{jj} response functions are given in the GRPA by

$$\chi_{nn}(\omega,Q)=e^2[P^{1,1}(\omega,Q)+P^{1,4}(\omega,Q)] + e^2[P^{4,1}(\omega,Q)+P^{4,4}(\omega,Q)] \quad (62)$$

and

$$\chi_{jj}(\omega,Q)=e^2v_F^2[P^{1,1}(\omega,Q)-P^{1,4}(\omega,Q)] + e^2v_F^2[-P^{4,1}(\omega,Q)+P^{4,4}(\omega,Q)], \quad (63)$$

respectively. We define an excitonic response function by

$$\chi_{\rm exc}(\omega,Q)=P^{2,2}(\omega,Q)+P^{3,3}(\omega,Q) \quad (64)$$

because $P^{2,2}(\omega,Q)$ and $P^{3,3}(\omega,Q)$ involve operators that create or destroy internodal electron-hole pairs.

If we sum over k in the GRPA equation, we get

$$I(\omega+i\delta)\overline{P}(\omega,Q)-\frac{1}{L_z}\sum_k[\overline{E}(k,Q)+\overline{\Sigma}(k)]\overline{P}_{k+Q,k}(\omega) -\frac{1}{L_z}\sum_k\overline{B}(k)\overline{H}(Q)\overline{P}(\omega,Q) +\frac{1}{L_z}\sum_{k'}\left[\frac{1}{L_z}\sum_k\overline{B}(k)\overline{X}(k-k')\right]\overline{P}_{k'+Q,k'}(\omega) =\frac{1}{L_z}\sum_k\overline{B}(k). \quad (65)$$

But, by the definition of the self-energy, we have the result

$$\frac{1}{L_z}\sum_k\overline{B}(k)\overline{X}(k-k')=\overline{\Sigma}(k'). \quad (66)$$

Thus, when performing a summation over k, the self-energies in the equation for $\overline{P}(\omega,Q)$ are exactly canceled by the vertex corrections due to the ladder diagrams. Moreover, since $e_\pm(k)-e_\pm(k+Q)=\pm\hbar v_FQ$ does not involve k, the summation over k gives directly (apart from a multiplicative constant), the responses $\chi_{nn}(\omega,Q)$ and $\chi_{jj}(\omega,Q)$. The same procedure cannot be applied to the excitonic response since $e_\pm(k)-e_\mp(k+Q)=(\mp2k\mp Q)\hbar v_F$ which is not just a function of Q. This cancellation is an example of a Ward identity and it occurs here because the noninteracting electronic dispersion is linear and the current operator has the special form $j_{z,\tau}=-e\tau v_F\sigma_z$ which is independent of k. We are thus left, for the components $P^{I,J}(\omega,Q)$, with $I,J=1,4$, (for $C=1$) with the equation

$$\begin{pmatrix}\omega+i\delta-v_zQ & -a_+(Q)H(Q)\\ -a_+(Q)H(Q) & \omega+i\delta+v_zQ\\ -a_-(Q)H(Q) & -a_-(Q)H(Q)\end{pmatrix} \times\begin{pmatrix}P^{1,1}(\omega,Q) & P^{1,4}(\omega,Q)\\ P^{4,1}(\omega,Q) & P^{4,4}(\omega,Q)\end{pmatrix} =\begin{pmatrix}a_+(Q) & 0\\ 0 & a_-(Q)\end{pmatrix}, \quad (67)$$

where we have defined

$$a_\pm(Q)=\frac{1}{2\pi\ell}\int_{-k_c\ell}^{+k_c\ell}dk\,\ell[\langle\rho_{\pm,\pm}(k+Q)\rangle-\langle\rho_{\pm,\pm}(k)\rangle]. \quad (68)$$

Note that, by symmetry,

$$a_+(Q)=-a_-(Q)=a(Q). \quad (69)$$

Solving Eq. (68) analytically, we arrive at the following results for the density and current responses:

$$\chi_{nn}(\omega,Q)=\frac{2e^2v_Fa(Q)Q}{(\omega+i\delta)^2-\frac{a(Q)}{Q\ell}\frac{v_F}{\ell}\frac{e^2}{\varepsilon_0\pi\hbar}-v_F^2Q^2} \quad (70)$$

and

$$\chi_{jj}(\omega, Q) = e^2 v_F^2 \frac{\frac{a^2(Q)}{Q^2\ell^2}\frac{2e^2}{\pi\varepsilon_0\hbar} + 2v_F a(Q)Q}{(\omega+i\delta)^2 - \frac{a(Q)}{Q\ell}\frac{v_F}{\ell}\frac{e^2}{\varepsilon_0\pi\hbar} - v_F^2Q^2}. \quad (71)$$

Both functions have a single pole at the plasmon frequency ω_p given by

$$\omega_p = \sqrt{\frac{a(Q)}{Q\ell}\frac{v_F}{\ell}\frac{e^2}{\varepsilon_0\pi\hbar} + v_F^2Q^2}. \quad (72)$$

In contrast, the proper responses $\widetilde{\chi}_{nn}(\omega, Q)$ and $\widetilde{\chi}_{jj}(\omega, Q)$ have a single pole at the intranodal electron-hole excitation $e_\pm(k) - e_\pm(k+Q) = \pm\hbar v_F Q$ of the noninteracting electron gas. This pole is transformed into the plasmon mode at a finite frequency by the Hartree term in the GRPA.

As we mentioned, the cancellation of the self-energy by the ladder diagrams does not occur for the excitonic response and we are thus forced to compute the full GRPA matrix equation numerically. This we do by discretizing the wave vector k in the exact same way as when solving the Hartree-Fock equation for the single-particle Green's function. We obtain a matrix equation that has the form

$$[I(\omega+i\delta) - \overline{\Upsilon}(k)]\overline{P}_{k+Q,k}(\omega) = \overline{B}(k), \quad (73)$$

where $\overline{\Upsilon}(k)$ is a $4(2N_p+1)\times 4(2N_p+1)$ matrix, with $2N_p+1$ the number of k values used in the HFA calculation.

VII. RESPONSE FUNCTIONS IN THE INCOHERENT STATE

In the incoherent but interacting ground state (doped or undoped), the function

$$a(Q) = \frac{Q}{2\pi} \quad (74)$$

so that the plasmon frequency is given exactly by

$$\omega_p = \sqrt{\frac{e^3 v_F B}{2\pi^2\varepsilon_0\hbar^2} + v_F^2Q^2} \quad (75)$$

which is the well-known result [23]. It does not depend on doping, nor on self-energy and vertex corrections. The density and current responses are exactly given by

$$\chi_{nn}(\omega, Q) = \frac{e^2 v_F Q^2/\pi}{(\omega+i\delta)^2 - \omega_p^2} \quad (76)$$

and

$$\chi_{jj}(\omega, Q) = e^2 v_F^2 \frac{\frac{e^3 B}{2\pi^3\varepsilon_0\hbar^2} + \frac{v_F Q^2}{\pi}}{(\omega+i\delta)^2 - \omega_p^2}, \quad (77)$$

respectively. They have a single pole at the plasmon frequency. As $Q\to 0$, the density response goes to zero but the current response remains finite. The coherences enter these response functions and the plasmon frequency only through the modification of the function $a(Q)$. Note that the continuum of excitations at $\omega = v_F Q$ has been transformed into the plasmon mode by the Hartree term (bubble diagrams) in the GRPA.

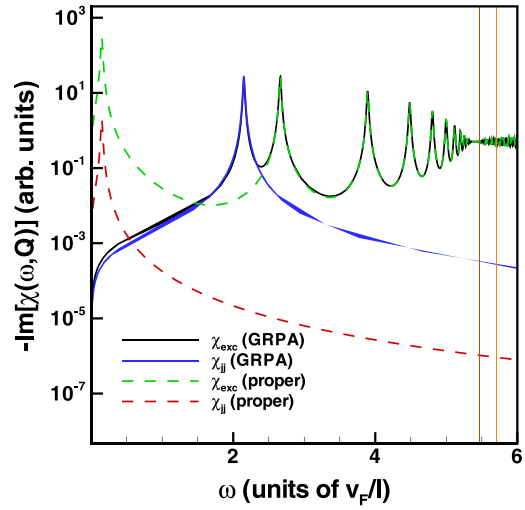

FIG. 9. Imaginary part of the excitonic and current response functions for $Q\ell = 0.15$ and $v_F/c = 0.001$ in the undoped coherent state. The full lines are the GRPA results while the dashed line are the proper responses. The vertical lines indicate the onset of the internodal continuum of electron-hole excitations (brown line) and the Hartree-Fock gap at $k = 0$ (orange line). The dielectric constant $\varepsilon_r = 1$.

In the absence of interaction and for $Q = 0$, the excitonic response $\chi_{\rm exc}^{(0)}$ is given by

$$\mathrm{Im}\left[-\chi_{\rm exc}^{(0)}(\omega, Q=0)\right] = \frac{1}{2v_F}\Theta(2v_F k_F - \omega) - \frac{1}{2v_F}\Theta(2v_F k_F + \omega) \quad (78)$$

and there is only a continuum of electron-hole pair excitations. With interaction but in the incoherent state where $\langle\rho_{-,+}(k)\rangle = 0$, the density and current responses are uncoupled from the excitonic response $\chi_{\rm exc}(\omega, Q)$. Moreover, the bubble diagrams do not contribute to $\chi_{\rm exc}(\omega, Q)$ in this case. The excitonic response is thus solution of the equation

$$\{(\omega+i\delta) - [\widetilde{e}_\mp(k) - \widetilde{e}_\pm(k+Q)]/\hbar\}P^\pm_{k+Q,k}(\omega) + \frac{e^2}{\varepsilon_0\hbar}b_\pm(k, Q)\frac{1}{L_z}\sum_q X(k-q)P^\pm_{q+Q,q}(\omega) = b_\pm(k, Q), \quad (79)$$

where we have defined

$$b_\pm(k, Q) = \langle\rho_{\pm,\pm}(k+Q)\rangle - \langle\rho_{\mp,\mp}(k)\rangle \quad (80)$$

and

$$\widetilde{e}_\tau(k) = e_\tau(k) + \Sigma_\tau(k). \quad (81)$$

The excitonic response in the GRPA is found by first solving Eq. (80) where the upper (lower) sign is for $P^{22}(P^{33})$ and then summing over k.

VIII. EXCITONIC RESPONSE IN THE COHERENT STATE WITH $C = 1$

Figure 9 shows the imaginary part of the excitonic and current response functions for $Q\ell = 0.15$ and $v_F/c = 0.001$

for nodes with Chern number $C = 1$. The full (dashed) line is the GRPA (proper) response. Since, in the current response, the ladder diagrams cancel the self-energies in Eq. (65), the proper responses $\widetilde{\chi}_{jj}(\omega, Q)$ and $\widetilde{\chi}_{nn}(\omega, Q)$ have only one pole which is at a frequency $\omega = [e_+(k) - e_+(k+Q)]/\hbar = v_F Q$ for $\omega \geqslant 0$. In the coherent phase, however, all response functions are coupled by the internodal coherence and so this mode also appears in $\widetilde{\chi}_{\rm exc}(\omega, Q)$ (the first peak in the green dashed line). The other peaks in $\widetilde{\chi}_{\rm exc}(\omega, Q)$ at energies E_n (with $n = 1, 2, \ldots$) are electron-hole bound states (excitons). Their energy increases with n until the energy of the electron-hole internodal continuum whose onset is $E_{\rm conti}(Q)$ is reached (this onset is indicated by the vertical brown line in Fig. 9). The bound-state energies for $Q \to 0$ are approximately given by $e_{B,n} = [E_{\rm conti}(Q) - E_1]/n^x$ where the exponent x depends on the Fermi velocity. Because of the vertex (ladder) corrections, the onset energy $E_{\rm conti}(Q)$ is slightly redshifted with respect to the Hartree-Fock gap $\Delta_{\rm HF}(Q) = E_+(Q) - E_-(0)$ indicated by the orange line in Fig. 9.

The gapless mode at $\omega = v_F Q$ is not a pole of $\widetilde{\chi}_{\rm exc}(\omega, Q)$ as calculated in the incoherent state using Eq. (80). It appears in $\widetilde{\chi}_{\rm exc}(\omega, Q)$ only in the coherent state. It is present in $\widetilde{\chi}_{jj}(\omega, Q)$ and $\widetilde{\chi}_{nn}(\omega, Q)$ as an intraband single-particle excitation but since it shows up in $\widetilde{\chi}_{\rm exc}(\omega, Q)$ as a gapless mode, we assume that it is also the collective mode related to the fluctuations of the global phase φ of the complex order parameter $\langle \rho_{-+} \rangle$. The series of excitonic bound states could then be associated with fluctuations in the amplitude of the order parameter. When the Hartree term is considered in calculating the GRPA response, this gapless mode is strongly renormalized and becomes gapped at the plasmon frequency given by Eq. (73). This frequency is slightly modified by the internodal coherence from its value in the incoherent phase which is given by Eq. (76). In contrast, the frequency of the excitonic peaks (the bound states) are almost unchanged when the Hartree term is switched on. In consequence, there is no gapless (Goldstone) mode in the GRPA spectrum of collective excitations for $\chi_{\rm exc}(\omega, Q)$ but there is one in the proper response. Similar results are obtained when the GRPA is applied to the study of collective excitations in superconductors [24,25].

Figure 10 shows the GRPA response functions $\chi_{jj}(\omega, Q)$ (blue line) and $\chi_{\rm exc}(\omega, Q)$ (black line) for $v_F/c = 0.002$ and $Q\ell = 0.015$. Again the plasmon appears as an extra pole in $\chi_{\rm exc}(\omega, Q)$ which is now in-between two bound states. As v_F/c increases and the Hartree-Fock gap decreases, the plasmon pole eventually ends up in the continuum of electron-hole internodal excitations.

Figure 11 shows $\chi_{jj}(\omega, Q)$ (blue line) and $\chi_{\rm exc}(\omega, Q)$ (black line) for $v_F/c = 0.001$ and $Q\ell = 0.15$ in the presence of electron doping. The Fermi wave vector is $k_F\ell = 0.1$. The excitonic response shows two bound states before the continuum of internodal electron-node excitations whose onset, indicated by the vertical brown line, would be at $\omega = [E_+(k_F) - E_-(k_F - Q)]/\hbar$ if vertex corrections were neglected but is actually increased by them. As in the undoped case, the excitonic response has an extra peak at the plasmon frequency. The series of peaks at low frequency in $\chi_{\rm exc}(\omega, Q)$ is the continuum of electron-hole excitations in the upper Hartree-Fock band (see Fig. 4) which extends from $\omega = [E_+(k_F) - E_+(k_F - Q)]/\hbar$ to $\omega = [E_+(k_F + Q) -$

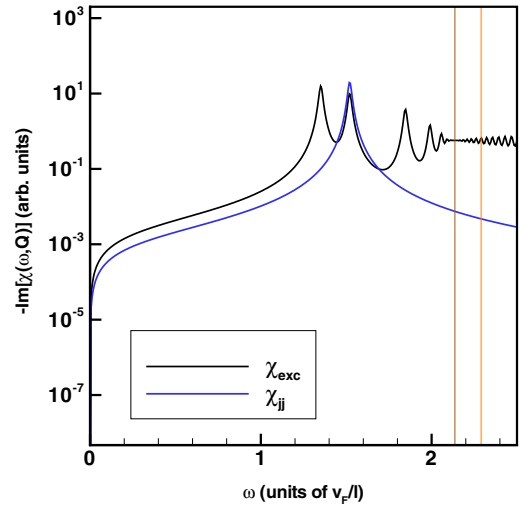

FIG. 10. Imaginary part of the GRPA excitonic (black curve) and current (blue curve) response functions for $Q\ell = 0.015$ and $v_F/c = 0.002$ in the undoped coherent phase. The vertical lines indicate the onset of the internodal electron-hole continuum (brown) and the Hartree-Fock gap at $k = 0$ (orange line). The dielectric constant $\varepsilon_r = 1$.

$E_+(k_F)]/\hbar$. As already noted, there is no continuum of excitations in $\chi_{jj}(\omega, Q)$ which has only the plasmon pole. For both continua in $\chi_{\rm exc}(\omega, Q)$, the peaks are due to our discretization of the wave vector k which is needed to solve the GRPA equations numerically.

IX. CONCLUSION

We have studied the effect of the long-range Coulomb interaction on the internodal coherence in a simple model of a two-node Weyl semimetal in the extreme quantum limit.

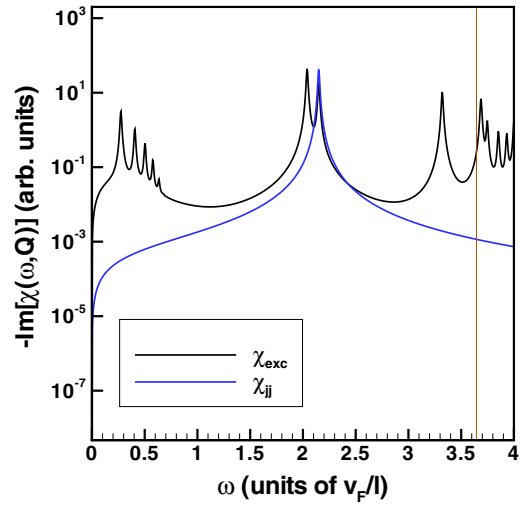

FIG. 11. Imaginary part of the GRPA excitonic and current response functions for $Q\ell = 0.15$ and $v_F/c = 0.002$ in the doped coherent state with Fermi wave vector $k_F\ell = 0.1$. The vertical brown line indicates the onset of the internode electron-hole continuum. The dielectric constant $\varepsilon_r = 1$.

We have considered Weyl nodes with Chern number $C = 1, 2, 3$. As our numerical calculations show, it is possible to find values of the Fermi velocity v_F, dielectric constant, and the doping level k_F where an excitonic condensate is possible and where the assumptions made to justify our model are satisfied. Nevertheless, the order parameter of the excitonic state decreases rapidly with the increase in all three parameters.

At the mean-field level, the main effect of the internodal electron-hole pairing is the opening of a gap in the chiral Landau levels making the system insulating. Our calculation assumes that the two nodes are two distinct systems and so this gap does not show up in the current or density response function where only a plasmon pole is present whose frequency is only slightly affected by the internodal coherence. If the two nodes are viewed as one system, then the excitonic state manifests itself as a charge-density wave in real space. The gap and the sliding motion of the CDW should then change the conductivity of the Weyl semimetal in several ways and cause anomalous magnetoelectric transport effects as discussed extensively in the literature (see Refs. [2–16]). At the moment of writing this paper, a few papers reported the experimental observation of an axionic CDW in the quasi-one-dimensional Weyl semimetal $(TaSe_4)_2I$ at zero magnetic field [15,29]. These claims are, however, under an active debate [30,31].

In our calculation, the excitonic response function shows a series of excitonic peaks in the gap opened by the internodal coherence. Their binding energy decreases until the electron-hole (internodal) continuum is reached. Because of the coupling between the different 16 response functions in the GRPA, an extra gapped mode also appears as a peak in the excitonic response function. In the proper excitonic response (ladder diagrams only), this peak is at the frequency $\omega = [e_\pm(k) - e_\pm(k+Q)]/\hbar = \pm v_F Q$ corresponding to a simple noninteracting intranodal electron-hole excitation. This frequency is pushed to the plasmon frequency when the full GRPA is computed by adding the bubble diagrams.

The presence of a magnetic field modifies profoundly the excitonic state with respect to its counterpart at zero magnetic field. The plasmon mode, the density modulation, and the Hartree-Fock gap (including its dependence on doping), which are in principle measurable quantities, all depend on the strength of the magnetic field. Equation (31) shows that the order parameter (and so the phase diagram) of the excitonic phase can be obtained from the amplitude of the density modulation. Another measurable observable of the coherent state is its magneto-optical spectrum. The optical absorption is related to the conductivity and to the proper part of the current response function: $\sigma_{zz}(\omega) = i\widetilde{\chi}_{zz}(\omega, q = 0)/\omega$. At the level of approximation made in our paper (keeping only the $n = 0$ chiral levels), there is no signature of the coherent state in absorption. More Landau levels need to be added to our model in order to see how the inter-Landau-level transitions are modified when coherence is present. This is not an easy task since more Landau levels also means more types of coherence such as internodal and/or inter-Landau-level. The size of the matrix that needs to be diagonalized in the calculation of the current response becomes rapidly out of hand. We leave this calculation for further work.

ACKNOWLEDGMENTS

R.C. was supported by a grant from the Natural Sciences and Engineering Research Council of Canada (NSERC) and S. F. Lopez by scholarhips from NSERC and the Fonds de recherche du Québec-Nature et technologies (FRQNT). Computer time was provided by the Digital Research Alliance of Canada.

APPENDIX A: HARTREE-FOCK FORMALISM FOR THE CALCULATION OF THE SINGLE-PARTICLE GREEN'S FUNCTION IN A COHERENT STATE

We give in this Appendix a summary of the Hartree-Fock formalism for the calculation of single-particle Green's function of a Weyl semimetal in a magnetic field and in the coherent state. We present the general case where an arbitrary number of Landau levels are considered and the Weyl nodes can have a Chern number $C = 1, 2, 3$. We allow for all types of coherence: internodal, inter-Landau-level, and complete entanglement

We consider a simple model of a Weyl semimetal (WSM) with broken time-reversal symmetry consisting of two nodes with Chern number C centered at wave vectors $\mathbf{b} = -\tau b\hat{\mathbf{z}}$ in momentum space and with opposite chiralities $\tau = \pm 1$. The noninteracting Hamiltonian for each node, written in the basis of the two bands that cross, is given by

$$h_\tau(\mathbf{k}) = \tau\hbar v_F \begin{pmatrix} k_z & \beta(k_x - ik_y)^C \\ \beta(k_x + ik_y)^C & -k_z \end{pmatrix}, \tag{A1}$$

where β is a material-dependent anisotropy factor, v_F is the Fermi velocity, and the wave vector $\mathbf{k}$ is restricted to a small region around each node.

We consider the WSM to be in a magnetic field $\mathbf{B} = \nabla \times \mathbf{A} = B\hat{\mathbf{z}}$. After making the Peierls substitution $\mathbf{k} \to \mathbf{k} + e\mathbf{A}/\hbar$ and working in the Landau gauge $\mathbf{A} = (0, Bx, 0)$, we can write

$$h_\tau(\mathbf{k}) = \tau v_F \begin{pmatrix} \hbar k_z & \beta\left(\frac{\sqrt{2}\hbar}{\ell}a\right)^C \\ \beta\left(\frac{\sqrt{2}\hbar}{\ell}a^\dagger\right)^C & -\hbar k_z \end{pmatrix}, \tag{A2}$$

where the ladder operators a, $a^\dagger$, which obey the commutation relation $[a, a^\dagger] = 1$, are defined by

$$a = \frac{\ell}{\sqrt{2}\hbar}(P_x - iP_y), \tag{A3}$$

$$a^\dagger = \frac{\ell}{\sqrt{2}\hbar}(P_x + iP_y), \tag{A4}$$

and where $\mathbf{P} = \hbar\mathbf{k} + e\mathbf{A}$ with $-e$ the electron charge.

We denote the different Landau levels by the set of indices (n, s, τ) where $n = 0, 1, 2, 3, \ldots$ and $s = \pm 1$ for the positive and negative energy levels. For the chiral (linearly dispersing levels), $s = +1$ only. For the nonchiral levels, the Landau-level dispersions are given by (to simplify the notation, we write k instead of k_z hereafter, the dispersion being along k_z only)

$$E_{n>0,s,k,\tau} = s\frac{\hbar v_F}{\ell}\sqrt{k^2\ell^2 + 2n},$$

$$E_{n>1,s,k,\tau} = s\frac{\hbar v_F}{\ell}\sqrt{k^2\ell^2 + 4\beta^2\left(\frac{\hbar}{\ell}\right)^2 n(n-1)},$$
$$E_{n>2,s,k,\tau} = s\frac{\hbar v_F}{\ell}\sqrt{k^2\ell^2 + 8\beta^2\left(\frac{\hbar}{\ell}\right)^4 n(n-1)(n-2)}, \tag{A5}$$

for $C = 1, 2, 3$, respectively, and the corresponding eigenvectors are given by

$$w_{n,s,k,X,\tau}(\mathbf{r},z) = \frac{1}{\sqrt{L_z}}\begin{pmatrix} u_{n,s,k,\tau}h_{n-C,X}(\mathbf{r}_\perp) \\ v_{n,s,k,\tau}h_{n,X}(\mathbf{r}_\perp)\end{pmatrix}e^{ikz}, \tag{A6}$$

where the factors

$$\begin{pmatrix} u_{n,s,k,\tau} \\ v_{n,s,k,\tau}\end{pmatrix} = \frac{1}{\sqrt{2}}\begin{pmatrix} s\tau(-i)^C\sqrt{1+\frac{\hbar\tau v_F k}{E_{n,s,k,\tau}}} \\ \sqrt{1-\frac{\hbar\tau v_F k}{E_{n,s,k,\tau}}}\end{pmatrix}. \tag{A7}$$

In these equations, X is the guiding-center index in the Landau gauge, $\mathbf{r}_\perp$ is a vector in the plane perpendicular to the magnetic field, and the factors and the functions $h_{n,X}(\mathbf{r}_\perp)$ are defined by

$$h_{n,X}(\mathbf{r}_\perp) = \varphi_n(x-X)e^{-iXy/\ell^2}/\sqrt{L_y}, \tag{A8}$$

where $\varphi_n(x)$ is a wave function of the one-dimensional harmonic oscillator.

There are C degenerate chiral levels at each node which we denote by the integer n ranging from $n = 0$ to $C-1$. They have the dispersion

$$e_\tau(k) = -\tau\frac{\hbar v_F}{\ell}k\ell. \tag{A9}$$

The corresponding eigenvectors are given by

$$w_{n,s,k,X,\tau}(\mathbf{r}) = \frac{1}{\sqrt{L_z}}\begin{pmatrix} 0 \\ h_{n,X}(\mathbf{r}_\perp)\end{pmatrix}e^{ikz}. \tag{A10}$$

They are the same for both nodes. Since the Landau-level energy is independent of the quantum number X, each state (n, s, k, τ) has degeneracy $N_\varphi = S/2\pi\ell^2$ where $S = L_xL_y$ is the area of the WSM perpendicular to the magnetic field. The volume of the WSM is $L_xL_yL_z$.

We write the field operator for each node in the basis of these eigenvectors so that

$$\Psi_\tau(\mathbf{r}) = \frac{1}{\sqrt{L_z}}\sum_{n,s,k,X}\begin{pmatrix} u_{n,s,k,\tau}h_{n-C,X}(\mathbf{r}_\perp) \\ v_{n,s,k,\tau}h_{n,X}(\mathbf{r}_\perp)\end{pmatrix}e^{ikz}c_{n,s,k,X,\tau}, \tag{A11}$$

where $c_{n,s,k,X,\tau}$ is the destruction operator for an electron in state (n, s, k, X, τ). The many-body Hamiltonian is then

$$H = \sum_\tau\int d^3r\,\Psi^\dagger_\tau(\mathbf{r})h_\tau(\mathbf{r})\Psi_\tau(\mathbf{r}) + \frac{1}{2}\sum_{\tau,\tau'}\int d^3r\int d^3r'\Psi^\dagger_\tau(\mathbf{r})\Psi^\dagger_{\tau'}(\mathbf{r}') \times V(\mathbf{r}-\mathbf{r}')\Psi_{\tau'}(\mathbf{r}')\Psi_\tau(\mathbf{r}), \tag{A12}$$

where the Coulomb interaction (in S. I. units)

$$V(\mathbf{r}) = \frac{1}{V}\sum_{\mathbf{q}}\frac{e^2}{\varepsilon_r\varepsilon_0|q_\perp^2+q_z^2|}e^{i\mathbf{q}_\perp\cdot\mathbf{r}_\perp}e^{iq_zz}, \tag{A13}$$

where the vector $\mathbf{q}_\perp = q_x\hat{\mathbf{x}} + q_y\hat{\mathbf{y}}$ and ε_r is the dielectric constant of the WSM. We remark that writing $e^{-i(\pm b+k)z}$ instead e^{ikz} in the field operators would make no change to H so that the internodal separation $2b$ does not enter our calculation. More precisely, we consider the two nodes as distinct systems. Another sequence for the field operators, namely, $\Psi^\dagger_\tau(\mathbf{u})\Psi^\dagger_{\tau'}(\mathbf{u}')\Psi_{-\tau'}(\mathbf{u}')\Psi_{-\tau}(\mathbf{u})$ with $\tau \neq \tau'$ could also be considered as it conserves the number of particles in each node. However, it leads to Fourier components of Coulomb interaction of the form $e^2/[\varepsilon_r\varepsilon_0(q_\perp^2 + (q_z \pm 2b)^2)]$. We assume that b is sufficiently large for these terms to be negligible in comparison with those that we keep.

In the (n, s, k, X, τ) basis, the Hamiltonian is given by

$$H = \sum_{t,k,X,\tau}E_{t,k,\tau}c^\dagger_{t,k,X,\tau}c_{t,k,X,\tau} + \frac{1}{2L_zS}\sum_{\mathbf{q}}\frac{e^2}{\varepsilon_0\varepsilon_r(q_\perp^2+q_z^2)}\sum_{\tau,\tau'}\sum_{k_1,k_2}\sum_{t_1,\ldots,t_4}\sum_{X_1,\ldots,X_4} \times\int d^2r_\perp w^\dagger_{t_1,k_1,X_1,\tau}(\mathbf{r}_\perp)e^{i\mathbf{q}_\perp\cdot\mathbf{r}_\perp}w_{t_4,k_1+q_z,X_4,\tau}(\mathbf{r}_\perp)\int d^2r'_\perp w^\dagger_{t_2,k_2,X_2,\tau'}(\mathbf{r}'_\perp)e^{-i\mathbf{q}_\perp\cdot\mathbf{r}'_\perp}w_{t_3,k_2-q_z,X_3,\tau'}(\mathbf{r}'_\perp) \times c^\dagger_{t_1,k_1,X_1,\tau}c^\dagger_{t_2,k_2,X_2,\tau'}c_{t_3,k_2-q_z,X_3,\tau'}c_{t_4,k_1+q_z,X_4,\tau}, \tag{A14}$$

where we have defined the superindex $t = (n, s)$ to lighten the notation. The matrix elements

$$\int d^2r_\perp w^\dagger_{t_1,k_1,X_1,\tau}(\mathbf{r}_\perp)e^{\pm i\mathbf{q}_\perp\cdot\mathbf{r}_\perp}w_{t_2,k_2,X_2,\tau}(\mathbf{r}_\perp) = e^{\pm\frac{i}{2}q_x(X_1+X_2)}\Lambda^{(\tau)}_{t_1,k_1;t_2,k_2}(\pm\mathbf{q}_\perp)\delta_{X_1,X_2\mp q_y\ell^2}, \tag{A15}$$

where we have defined

$$\Lambda^{(\tau)}_{t_1,k_1;t_2,k_2}(\mathbf{q}_\perp) = u^*_{t_1,k_1,\tau}u_{t_2,k_2,\tau}F_{n_1-1,n_2-1}(\mathbf{q}_\perp) + v^*_{t_1,k_1,\tau}v_{t_2,k_2,\tau}F_{n_1,n_2}(\mathbf{q}_\perp),\ \text{if } n_1, n_2 \geqslant C$$
$$\Lambda^{(\tau)}_{t_1,k_1;t_2,k_2}(\mathbf{q}_\perp) = v^*_{t_1,k_1,\tau}F_{n_1,n_2}(\mathbf{q}_\perp),\ \text{if } n_1 \geqslant C \text{ and } n_2 < C$$
$$\Lambda^{(\tau)}_{t_1,k_1;t_2,k_2}(\mathbf{q}_\perp) = v_{t_2,k_2,\tau}F_{n_1,n_2}(\mathbf{q}_\perp),\ \text{if } n_2 \geqslant C \text{ and } n_1 < C$$
$$\Lambda^{(\tau)}_{t_1,k_1;t_2,k_2}(\mathbf{q}_\perp) = F_{n_1,n_2}(\mathbf{q}_\perp),\ \text{if } n_1, n_2 < C \tag{A16}$$

and the function

$$F_{n_1,n_2}(\mathbf{q}_\perp) = \sqrt{\frac{\mathrm{Min}(n_1,n_2)!}{\mathrm{Max}(n_1,n_2)!}}\left(\frac{iq_\perp\ell}{\sqrt{2}}\right)^{|n_1-n_2|} e^{-i(n_1-n_2)\theta} L^{|n_1-n_2|}_{\mathrm{Min}(n_1,n_2)}\left(\frac{q_\perp^2\ell^2}{2}\right) e^{-\frac{q_\perp^2\ell^2}{4}}, \tag{A17}$$

where θ is the angle between the vector $\mathbf{q}_\perp$ and the x axis and $L_n^m(x)$ is a generalized Laguerre polynomial.

At this point, we define the operators

$$\rho_{t,k,\tau;t',k',\tau'}(\mathbf{q}_\perp) \equiv \frac{1}{N_\varphi}\sum_{X,X'} e^{-\frac{i}{2}q_x(X+X')}\delta_{X,X'+q_y\ell^2} c^\dagger_{t,k,X,\tau} c_{t',k',X',\tau'}. \tag{A18}$$

The set of averages $\{\langle\rho_{t,k,\tau;t',k',\tau'}(\mathbf{q}_\perp)\rangle\}$ define any phase of the electron gas in the WSM whether uniform or modulated spatially and with any type of coherences: internodal, inter-Landau-level, or complete entanglement.

After making the Hartree-Fock pairing of the operators in the interacting Hamiltonian, we get

$$\begin{aligned} H_{\mathrm{HF}} = {} & N_\varphi \sum_{t,k,\tau} E_{t,k,\tau}\rho_{t,k,\tau;t,k,\tau}(0) + \frac{N_\varphi^2}{L_z}\sum_{\mathbf{q}}\sum_{\tau,\tau'}\sum_{k_1,k_2}\sum_{t_1,\ldots,t_4} H^{(\tau,\tau')}_{t_1,k_1;t_4,k_1+q_z;t_2,k_2;t_3,k_2-q_z}(\mathbf{q})\langle\rho_{t_1,k_1,\tau;t_4,k_1+q_z,\tau}(-\mathbf{q}_\perp)\rangle\rho_{t_2,k_2,\tau';t_3,k_2-q_z,\tau'}(\mathbf{q}_\perp) \\ & - \frac{N_\varphi}{L_z}\sum_{\mathbf{q}}\sum_{\tau,\tau'}\sum_{k_1,k_2}\sum_{t_1,\ldots,t_4} X^{(\tau,\tau')}_{t_1,k_1;t_4,k_1+q_z;t_2,k_2;t_3,k_2-q_z}(\mathbf{q})\langle\rho_{t_1,k_1,\tau;t_3,k_2-q_z,\tau'}(-\mathbf{q}_\perp)\rangle\rho_{t_2,k_2,\tau';t_4,k_1+q_z,\tau}(\mathbf{q}_\perp), \end{aligned} \tag{A19}$$

where $\mathbf{t}_\perp = t_x\widehat{\mathbf{x}} + t_y\widehat{\mathbf{y}}$ and the Hartree and Fock interactions are given by

$$H^{(\tau,\tau')}_{t_1,k_1;t_2,k_2;t_3,k_3;t_4,k_4}(\mathbf{q}) = \frac{1}{S}\Lambda^{(\tau)}_{t_1,k_1;t_2k_2}(\mathbf{q}_\perp)V(\mathbf{q})\Lambda^{(\tau')}_{t_3k_3;t_4,k_4}(-\mathbf{q}_\perp), \tag{A20}$$

$$X^{(\tau,\tau')}_{t_1,k_1;t_2,k_2;t_3,k_3;t_4,k_4}(\mathbf{q}) = \frac{1}{S}\sum_{\mathbf{t}_\perp} e^{-i\mathbf{t}_\perp\times\mathbf{q}_\perp\ell^2}\Lambda^{(\tau)}_{t_1,k_1;t_2,k_2}(\mathbf{t}_\perp)V(\mathbf{t}_\perp,q_z)\Lambda^{(\tau')}_{t_3,k_3;t_4,k_4}(-\mathbf{t}_\perp). \tag{A21}$$

To compute the $\langle\rho_{t,k,\tau;t',k',\tau'}(\mathbf{q}_\perp)\rangle$'s, we define the single-particle Matsubara Green's function

$$G_{t,k,\tau;t',k',\tau'}(\mathbf{q}_\perp;\tau_0) = \frac{1}{N_\varphi}\sum_{X,X'} e^{-\frac{i}{2}q_x(X+X')}\delta_{X,X'-q_y\ell^2} G_{t,k,\tau;t',k',\tau'}(X,X';\tau_0), \tag{A22}$$

where the imaginary-time Green's function is defined as

$$G_{t,k,\tau;t',k',\tau'}(X,X';\tau_0) = -\langle T_{\tau_0} c_{t,k,X,\tau}(\tau_0) c^\dagger_{t',k',X',\tau'}(0)\rangle, \tag{A23}$$

with T_{τ_0} the imaginary-time ordering operator and τ_0 the imaginary time (not to be confused with the node index). When $\tau_0 = 0^-$,

$$G_{t,k,\tau;t',k',\tau'}(\mathbf{q}_\perp;\tau_0 = 0^-) = \langle\rho_{t',k',\tau';t,k,\tau}(\mathbf{q}_\perp)\rangle. \tag{A24}$$

Now, using the Fourier transform

$$G_{t,k,\tau;t',k',\tau'}(\mathbf{q}_\perp, i\omega_m) = \int_0^{\beta\hbar} d\tau_0 e^{i\omega_m\tau_0} G_{t,k,\tau;t',k',\tau'}(\mathbf{q}_\perp,\tau_0), \tag{A25}$$

with the Matsubara fermionic frequencies

$$\omega_m = \frac{(2m+1)\pi}{\beta\hbar}, \qquad m = 0, \pm1, \pm2, \ldots \tag{A26}$$

and $\beta = 1/k_BT$ with T the temperature and k_B the Boltzmann constant, we finally obtain the sought averages by performing the Matsubara frequency sum

$$\langle\rho_{t',k',\tau';t,k,\tau}(\mathbf{q}_\perp)\rangle = \frac{1}{\beta\hbar}\sum_{i\omega_m} e^{-i\omega_m 0^-} G_{t,k,\tau;t',k',\tau'}(\mathbf{q}_\perp, i\omega_m). \tag{A27}$$

It remains to derive the Hartree-Fock equation for the Green's function $G_{t,k,\tau;t',k',\tau'}(\mathbf{q}_\perp, i\omega_m)$. This is done by using the Heisenberg equation of motion

$$\hbar\frac{\partial}{\partial\tau_0}(\ldots) = [H - \mu N_e, (\ldots)], \tag{A28}$$

where μ is the chemical potential and N_e the electron-number operator. After a long calculation, we get

$$\left[i\omega_n - \frac{1}{\hbar}(E_{t,k,\tau} - \mu)\right] G_{t,k,\tau;t',k',\tau'}(\mathbf{q}_\perp, i\omega_n)$$

$$= \delta_{\tau,\tau'}\delta_{t,t'}\delta_{k,k'}\delta_{\mathbf{q}_\perp,0} + \frac{N_\varphi}{\hbar L_z}\sum_{\mathbf{q}'}\sum_{\tau''}\sum_{k_1}\sum_{t_1,t_3,t_4} H^{(\tau'',\tau)}_{t_1,k_1;t_4,k_1+q'_z;t,k;t_3,k-q'_z}(\mathbf{q}'_\perp - \mathbf{q}_\perp, q'_z)\langle\rho_{t_1,k_1,\tau'';t_4,k_1+q'_z,\tau''}(\mathbf{q}_\perp - \mathbf{q}'_\perp)\rangle$$
$$\times e^{-\frac{i}{2}(\mathbf{q}_\perp\times\mathbf{q}'_\perp)\ell^2\cdot\hat{\mathbf{z}}} G_{t_3,k-q'_z,\tau;t',k',\tau'}(\mathbf{q}'_\perp;\omega_n)$$
$$- \frac{1}{\hbar L_z}\sum_{\mathbf{q}'}\sum_{\tau''}\sum_{k_1}\sum_{t_1,t_3,t_4} X^{(\tau'',\tau)}_{t_1,k_1;t_4,k_1+q'_z;t,k;t_3,k-q'_z}(\mathbf{q}'_\perp - \mathbf{q}_\perp, q'_z)\langle\rho_{t_1,k_1,\tau'';t_3,k-q'_z,\tau}(\mathbf{q}_\perp - \mathbf{q}'_\perp)\rangle$$
$$\times e^{-\frac{i}{2}(\mathbf{q}_\perp\times\mathbf{q}'_\perp)\ell^2\cdot\hat{\mathbf{z}}} G_{t_4,k_1+q'_z,\tau'';t',k',\tau'}(\mathbf{q}'_\perp;\omega_n). \tag{A29}$$

The average of the electronic density is given by

$$\langle n_e(\mathbf{q})\rangle = \sum_\tau \int d^3r \langle\Psi^\dagger_\tau(\mathbf{r})e^{-i\mathbf{q}\cdot\mathbf{r}}\Psi_\tau(\mathbf{r})\rangle = N_\varphi \sum_{\tau,t,t',k} \Lambda^{(\tau)}_{t,k;t',k+q_z}(-\mathbf{q}_\perp)\langle\rho_{t,k,\tau;t',k+q_z,\tau}(\mathbf{q}_\perp)\rangle \tag{A30}$$

an so in the particular case where the electron gas is not modulated spatially, we must have $\langle n_e(\mathbf{q})\rangle \neq 0$ for $q = 0$ only which implies that

$$\langle\rho_{t',k',\tau';t,k,\tau}(\mathbf{q}_\perp)\rangle = \langle\rho_{t',k,\tau';t,k,\tau}(0)\rangle\delta_{k,k'}\delta_{\mathbf{q}_\perp,0}. \tag{A31}$$

This condition simplifies the Hamiltonian which becomes

$$H_{\mathrm{HF}} = N_\varphi \sum_{t,k,\tau} E_{t,k,\tau}\rho^{(\tau,\tau)}_{t,t}(k) - \frac{N_\varphi}{L_z}\sum_{\tau,\tau'}\sum_{k_1,k_2}\sum_{t_1,\ldots,t_4} X^{(\tau,\tau')}_{t_1,k_1;t_4,k_2;t_2,k_2;t_3,k_1}(q_z = k_2 - k_1)\left\langle\rho^{(\tau,\tau')}_{t_1,t_3}(k_1)\right\rangle\rho^{(\tau',\tau)}_{t_2,t_4}(k_2) \tag{A32}$$

and the equation for the single-particle Green's function also simplifies to

$$\left[i\omega_n - \frac{1}{\hbar}(E_{t,\tau}(k) - \mu)\right]G^{(\tau,\tau')}_{t,t'}(k, i\omega_n) - \frac{1}{\hbar}\sum_{\tau'',t''}\Sigma^{(\tau,\tau'')}_{t,t''}(k)G^{(\tau'',\tau')}_{t'',t'}(k, i\omega_n) = \delta_{\tau,\tau'}\delta_{t,t'}, \tag{A33}$$

where we have defined the Fock self-energy

$$\Sigma^{(\tau,\tau')}_{t,t'}(k) = -\frac{1}{L_z}\sum_{k_1}\sum_{t_1,t_2} X^{(\tau',\tau)}_{t_1,k_1;t',k;t,k;t_2,k_1}(0, k - k_1)\left\langle\rho^{(\tau',\tau)}_{t_1,t_2}(k_1)\right\rangle \tag{A34}$$

and simplified the notation to

$$G^{(\tau,\tau')}_{t,t'}(k, i\omega_n) = G_{t,k,\tau;t',k,\tau'}(\mathbf{q}_\perp = 0, i\omega_n), \tag{A35}$$

$$\left\langle\rho^{(\tau,\tau')}_{t,t'}(k)\right\rangle = \langle\rho_{t,k,\tau;t',k,\tau'}(\mathbf{q}_\perp = 0)\rangle. \tag{A36}$$

In a uniform state, the Hartree term is canceled by the positive ionic background of the WSM and so there is no Hartree self-energy. The Hartree-Fock equation of motion for $G^{(\tau,\tau')}_{t,t'}(k, i\omega_n)$ is a self-consistent equation since the self-energy contains the very averages that we want to compute.

Defining the superindices $I, J, K = (t, \tau) = 1, 2, 3, \ldots, N$ where N is the total number of levels considered, Eq. (A33) can be written as

$$\sum_K [i\omega_n\delta_{I,K} - F_{I,K}(k)]G_{K,J}(k, i\omega_n) = \delta_{I,J}, \tag{A37}$$

where the matrix

$$F_{I,J}(k) = \frac{1}{\hbar}\{[E_{t,\tau}(k) - \mu]\delta_{I,J} - \Sigma_{I,J}(k)\}. \tag{A38}$$

Because of the symmetry relations

$$\langle\rho_{I,J}(k)\rangle = \langle\rho_{J,I}(k)\rangle^*, \tag{A39}$$

$$F_{n,n'}(\mathbf{q}_\perp) = [F_{n',n}(-\mathbf{q}_\perp)]^*, \tag{A40}$$

$$\Lambda^{(\tau)}_{t,k;t'k'}(\mathbf{q}_\perp) = \left[\Lambda^{(\tau)}_{t',k';t,k}(-\mathbf{q}_\perp)\right]^*, \tag{A41}$$

it follows that

$$H^{(\tau,\tau')}_{t_1,k_1;t_2,k_2;t_3,k_3;t_4,k_4}(\mathbf{q}) = \left[H^{(\tau',\tau)}_{t_4,k_4;t_3,k_3;t_2,k_2;t_1,k_1}(-\mathbf{q})\right]^*,$$
$$X^{(\tau,\tau')}_{t_1,k_1;t_2,k_2;t_3,k_3;t_4,k_4}(\mathbf{q}) = \left[X^{(\tau',\tau)}_{t_4,k_4;t_3,k_3;t_2,k_2;t_1,k_1}(-\mathbf{q})\right]^* \tag{A42}$$

and for the self-energies

$$\Sigma^{(\tau,\tau')}_{t,t'}(k) = \left[\Sigma^{(\tau',\tau)}_{t',t}(k)\right]^*. \tag{A43}$$

Thus, $F_{I,J}(k)$ is a Hermitian matrix that can be diagonalized by a unitary transformation. In matrix form,

$$F(k) = U(k)D(k)U^\dagger(k), \tag{A44}$$

where $U(k)$ is the matrix of the eigenvectors of $F(k)$ and $D(k)$ the diagonal matrix of its real eigenvalues $d_m(k)$ where $m = 1, 2, \ldots, N$. The Green's functions are given by

$$G_{I,J}(k, i\omega_n) = \sum_{m=1}^{N}\frac{U_{I,m}(k)[U^\dagger(k)]_{m,J}}{i\omega_n + \mu/\hbar - d_m(k)}. \tag{A45}$$

Performing the Matsubara frequency sum, we get, at $T = 0$ K, that the ground-state averages are given by

$$\langle\rho_{J,I}(k)\rangle = \sum_{m=1}^{N} U_{I,m}(k)[U^\dagger(k)]_{m,J}\Theta[e_F - d_m(k)], \tag{A46}$$

where e_F is the Fermi level which is determined by the relation

$$\sum_I\sum_k\langle\rho_{I,I}(k)\rangle = \sum_k\sum_{m=1}^{N}\Theta[e_F - d_m(k))] = N_e, \tag{A47}$$

where N_e is the number of electrons in the two nodes.

In the approximation where we consider only the chiral levels in the Hilbert space and where the state is uniform spatially, we have the simplification

$$\Lambda^{(\tau)}_{t_1,k_1;t_2,k_2}(\mathbf{q}_\perp) = F_{n_1,n_2}(\mathbf{q}_\perp), \tag{A48}$$

with the integers n_1, n_2 ranging from 0 to $C-1$ and with $t_1 = n_1, t_2 = n_2$ since $s_1 = s_2 = 1$. The interactions are then given by

$$X^{(\tau,\tau')}_{n_1,n_2,n_3,n_4}(\mathbf{q}_\perp = 0, q_z) = \frac{e^2}{\varepsilon_0\varepsilon_r}\int_0^{+\infty}\frac{dt_\perp \ell}{(2\pi)^2}\frac{t_\perp \ell}{t_\perp^2\ell^2 + q_z^2\ell^2} \times \int_0^{2\pi} d\theta\, F_{n_1,n_2}(\mathbf{t}_\perp\ell)F_{n_3,n_4}(-\mathbf{t}_\perp\ell), \tag{A49}$$

where θ is the angle between the vector $\mathbf{t}_\perp$ and the x axis. They do not depend on the chirality index nor on the vectors $k_1, \ldots, k_4$. The angular part is $\int_0^{2\pi} d\theta\, e^{-i(n_1-n_2+n_3-n_4)\theta}$ and is finite only if $n_1 - n_2 + n_3 - n_4 = 0$. The nonzero interactions are thus given by

$$X_{n_1,n_2,n_3,n_4}(x) = \frac{e^2}{2\pi\varepsilon_0\varepsilon_r}\sqrt{\frac{\mathrm{Min}(n_1,n_2)!}{\mathrm{Max}(n_1,n_2)!}}\sqrt{\frac{\mathrm{Min}(n_3,n_4)!}{\mathrm{Max}(n_3,n_4)!}} \times \int_0^{+\infty} dy \frac{y}{y^2+x^2}\left(\frac{y}{\sqrt{2}}\right)^{|n_1-n_2|+|n_3-n_4|} \times i^{|n_1-n_2|-|n_3-n_4|}L^{|n_1-n_2|}_{\mathrm{Min}(n_1,n_2)}\left(\frac{y^2}{2}\right)L^{|n_3-n_4|}_{\mathrm{Min}(n_3,n_4)} \times \left(\frac{y^2}{2}\right)e^{-\frac{y^2}{2}}. \tag{A50}$$

They have the form X_{n_1,n_2,n_2,n_1} or X_{n_1,n_1,n_2,n_2} for $C = 1, 2$. For $C = 3$, one must add to these terms the four terms $X_{2,1,0,1}, X_{1,2,1,0}, X_{0,1,2,1}, X_{1,0,1,2}$. Thus, there are 1, 6, and 19 nonzero interactions for $C = 1, 2, 3$, respectively. They are, however, not all different as shown in Appendix B.

APPENDIX B: FOCK INTERACTIONS FOR $C = 1, 2, 3$

The nonzero Fock interactions, defined in Eq. (A50), are given by ($x = k\ell$ and $\alpha = e^2/2\pi\varepsilon_0\varepsilon_r$) the following.

1. $C = 1$

$$X_{0,0,0,0}(x) = \alpha\frac{1}{2}e^{\frac{x^2}{2}}\Gamma\left(0, \frac{x^2}{2}\right). \tag{B1}$$

2. $C = 2$

The above result and

$$X_{1,1,1,1}(x) = \alpha\frac{1}{8}(2+x^2)\left[-2 + (2+x^2)e^{\frac{x^2}{2}}\Gamma\left(0, \frac{x^2}{2}\right)\right], \tag{B2}$$

$$X_{0,0,1,1}(x) = X_{1,1,0,0}(x) = \alpha\frac{1}{4}\left[-2 + (2+x^2)e^{\frac{x^2}{2}}\Gamma\left(0, \frac{x^2}{2}\right)\right], \tag{B3}$$

$$X_{0,1,1,0}(x) = X_{1,0,0,1}(x) = \alpha\frac{1}{2}\left[1 - \frac{1}{2}x^2e^{\frac{x^2}{2}}\Gamma\left(0, \frac{x^2}{2}\right)\right]. \tag{B4}$$

3. $C = 3$

All of the above results and

$$X_{0,0,2,2}(x) = X_{2,2,0,0}(x) = \alpha\frac{1}{16}\left[-12 - 2x^2 + (8 + 8x^2 + x^4)e^{\frac{x^2}{2}}\Gamma\left(0, \frac{x^2}{2}\right)\right], \tag{B5}$$

$$X_{1,1,2,2}(x) = X_{2,2,1,1}(x) = \alpha\frac{1}{32}(2+x^2)\left[-12 - 2x^2 + (8 + 8x^2 + x^4)e^{\frac{x^2}{2}}\Gamma\left(0, \frac{x^2}{2}\right)\right],$$

$$X_{2,2,2,2}(x) = \alpha\frac{1}{128}(8 + 8x^2 + x^4)\left[-12 - 2x^2 + (8 + 8x^2 + x^4)e^{\frac{x^2}{2}}\Gamma\left(0, \frac{x^2}{2}\right)\right], \tag{B6}$$

and

$$X_{0,2,2,0}(x) = X_{2,0,0,2}(x) = \alpha\frac{1}{16}\left[4 - 2x^2 + x^4e^{\frac{x^2}{2}}\Gamma\left(0, \frac{x^2}{2}\right)\right], \tag{B7}$$

$$X_{1,2,2,1}(x) = X_{2,1,1,2}(x) = \alpha\frac{1}{32}(4+x^2)\left[4 + 2x^2 - (4x^2 + x^4)e^{\frac{x^2}{2}}\Gamma\left(0, \frac{x^2}{2}\right)\right], \tag{B8}$$

and

$$X_{2,1,0,1}(x) = X_{1,2,1,0}(x) = X_{0,1,2,1}(x) = X_{1,0,1,2}(x)$$
$$= \alpha \frac{1}{8\sqrt{2}} \left[4 + 2x^2 - (4x^2 + x^4) e^{\frac{x^2}{2}} \Gamma\left(0, \frac{x^2}{2}\right) \right]. \tag{B9}$$

[1] For a review of Weyl semimetals, see, for example, P. Hosur, and X.-L. Qi, Recent developments in transport phenomena in Weyl semimetals, C. R. Phys. **14**, 857 (2013); N. P. Armitage, E. J. Mele, A. Vishwanath, Weyl and Dirac semimetals in three-dimensional solids, Rev. Mod. Phys. **90**, 015001 (2018).

[2] K.-Y. Yang, Y-M. Lu, and Y. Ran, Quantum Hall effects in a Weyl semimetal: Possible application in pyrochlore iridates, Phys. Rev. B **84**, 075129 (2011).

[3] A. A. Zyuzin and A. A. Burkov, Topological response in Weyl semimetals and the chiral anomaly, Phys. Rev. B **86**, 115133 (2012).

[4] H. Wei, S.-P. Chao, and V. Aji, Excitonic phases from Weyl semimetals, Phys. Rev. Lett. **109**, 196403 (2012).

[5] Z. Wang and S. C. Zhang, Chiral anomaly, charge density waves, and axion strings from Weyl semimetals, Phys. Rev. B **87**, 161107(R) (2013).

[6] H. Wei, S.-P. Chao, and V. Aji, Long-range interaction induced phases in Weyl semimetals, Phys. Rev. B **89**, 235109 (2014).

[7] J. Maciejko and R. Nandkishore, Weyl semimetals with short-range interactions, Phys. Rev. B **90**, 035126 (2014).

[8] V. A. Miranky and I. A. Shovkovy, Quantum field theory in a magnetic field: From quantum chromodynamics to graphene and Dirac semimetals, Phys. Rep. **576**, 1 (2015).

[9] B. Roy and J. D. Sau, Magnetic catalysis and axionic charge density wave in Weyl semimetals, Phys. Rev. B **92**, 125141 (2015).

[10] B. Roy, P. Goswami, and V. Juričić, Interacting Weyl fermions: Phases, phase transitions, and global phase diagram, Phys. Rev. B **95**, 201102(R) (2017).

[11] X. Li, B. Roy, and S. Das Sarma, Weyl fermions with arbitrary monopoles in magnetic fields: Landau levels, longitudinal magnetotransport, and density-wave ordering, Phys. Rev. B **94**, 195144 (2016).

[12] Z. Song, Z. Fang, and X. Dai, Instability of Dirac semimetal phase under a strong magnetic field, Phys. Rev. B **96**, 235104 (2017).

[13] N. S. Srivatsa and R. Ganesh, Excitonic collective modes in Weyl semimetals, Phys. Rev. B **98**, 165133 (2018).

[14] F. Xue and X.-X. Zhang, Instability and topological robustness of Weyl semimetals against Coulomb interaction, Phys. Rev. B **96**, 195160 (2017).

[15] J. Gooth, B. Bradlyn, S. Honnali, C. Schindler, N. Kumar, J. Noky, Y. Qi, C. Shekhar, Y. Sun, Z. Wang, B. A. Bernevig, and C. Felser, Axionic charge-density wave in the Weyl semimetal $(TaSe_4)_2$ I, Nature (London) **575**, 315 (2019).

[16] J. B. Curtis, I. Petrides, and Prineha Narang, Finite-momentum instability of a dynamical axion insulator, Phys. Rev. B **107**, 205118 (2023).

[17] R. Kundu, H. A. Fertig, and A. Kundu, Broken symmetry and competing orders in Weyl semimetal interfaces, Phys. Rev. B **107**, L041402 (2023).

[18] E. Mottola, A. V. Sadofyev, and A. Stergiou, Axions and superfluidity in Weyl semimetals, Phys. Rev. B **109**, 134512 (2024).

[19] J. Bernabeu and A. Cortijo, Chiral symmetry restoration and the ultraquantum limit of axionic charge density waves in Weyl semimetals, J. High Energy Phys. 03 (2024) 126.

[20] R. D. Peccei and H. R. Quinn, CP conservation in the presence of pseudoparticles, Phys. Rev. Lett. **38**, 1440 (1977).

[21] F. Wilczek, Two applications of axion electrodynamics, Phys. Rev. Lett. **58**, 1799 (1987).

[22] J. R. Tolsma, F. Wu, A. H. MacDonald, Collective modes of Dirac and Weyl semimetals in strong magnetic fields, arXiv:1710.02171.

[23] See, for example, S. Das Sarma, and E. H. Hwang, Collective modes of the massless Dirac plasma, Phys. Rev. Lett. **102**, 206412 (2009); D. T. Son and B. Z. Spivak, Chiral anomaly and classical negative magnetoresistance of Weyl metals, Phys. Rev. B **88**, 104412 (2013); M. Lv and S. C. Zhang, Dielectric function, Friedel oscillation and plasmons in Weyl semimetals, Int. J. Mod. Phys. B **27**, 1350177 (2013); J. Hofmann and S. Das Sarma, Plasmon signature in Dirac-Weyl liquids, Phys. Rev. B **91**, 241108(R) (2015).

[24] P. W. Anderson, Random-phase approximation in the theory of superconductivity, Phys. Rev. **112**, 1900 (1958).

[25] A. Bardasis and J. R. Schrieffer, Excitons and plasmons in superconductors, Phys. Rev. **121**, 1050 (1961).

[26] K. Jia, J. Yao, X. He, Y. Li, J. Deng, M. Yang, J. Wang, Z. Zhu, C. Wang, D. Yan, H. L. Feng, J. Shen, Y. Luo, Z. Wang, and Y. Shi, Discovery of a magnetic topological semimetal $Eu_3In_2As_4$ with a single pair of Weyl points, arXiv:2403.07637.

[27] L. P. Kadanoff and G. Baym, *Quantum Statistical Mechanics* (Benjamin, New York, 1962); G. Baym and L. P. Kadanoff, Conservation laws and correlation functions, Phys. Rev. **124**, 670 (1961); G. Baym, Self-consistent approximations in many-body systems, *ibid.* **127**, 1391 (1962).

[28] S. Bertrand, J.-M. Parent, R. Côté, and I. Garate, Complete optical valley polarization in Weyl semimetals in strong magnetic fields, Phys. Rev. B **100**, 075107 (2019).

[29] W. Shi, B. J. Wieder, H. L. Meyerheim, Y. Sun, Y. Zhang, Y. Li, L. Shen, Y. Qi, L. Yang, J. Jena, P. Werner, K. Koepernik, S. Parkin, Y. Chen, C. Felser, B. A. Bernevig, and Z. Wang, A charge-density-wave topological semimetal, Nat. Phys. **17**, 381 (2021).

[30] A. A. Sinchenko, R. Ballou, J. E. Lorenzo, Th. Grenet, and P. Monceau, Does $(TaSe_4)_2$ I really harbor an axionic charge density wave? Appl. Phys. Lett. **120**, 063102 (2022).

[31] Z. Huang, H. Yi, L. Min, Z. Mao, C.-Z. Chang, and W. Wu, Absence of in-gap modes in charge density wave edge dislocations of the Weyl semimetal $(TaSe_4)_2$ I, Phys. Rev. B **104**, 205138 (2021).